SMALL-ANIMAL SPECT/CT AND NANOFIBRILLAR CELLULOSE HYDROGELS: A PRECLINICAL EVALUATION OF A POTENTIAL NOVEL BIOMATERIAL APPLICATION

Patrick Laurén
University of Helsinki
Faculty of Pharmacy
The Division of
Biopharmaceutics and
Pharmacokinetics

March 2013

TABLE OF CONTENTS

1 INTRODUCTION 01
2 CELLULOSE NANOFIBERS 02
2.1 Properties 02
2.2 Biomaterial research 05
2.3 Applications 07
2.3.1 Bacterial cellulose 08
2.3.2 Plant-derived cellulose 10
2.4 Future perspectives 12
3 SPECT/CT 13
3.1 Single-photon emission computed tomography 13
3.2 Multimodality 17
3.3 Advantages & limitations 18
3.4 Single photon-emitting radionuclides 20
3.4.1 Technetium-99m 21
3.4.2 Iodine-123 21
3.4.3 Other radionuclides 22
3.5 Radiation safety 22
3.5.1 Regulatory issues 23
3.5.2 Activity and exposure 24
3.5.3 Radiation detriment 26
3.6 Translational aspects 28
3.6.1 Clinical SPECT/CT 28
3.6.2 Small-animal SPECT/CT 29
3.7 Imaging as a tool for biopharmaceutical research 31
4 AIMS OF THE STUDY 33
5 MATERIALS & METHODS 34
5.1 Diffusion study 34
5.2 ^{99m}Tc-NFC labelling 34
5.3 *In vivo* imaging 35
6 RESULTS 37
6.1 Diffusion study 37
6.2 ^{99m}Tc-NFC labelling 38
6.3 *In vivo* imaging 43
7 DISCUSSION 54
8 CONCLUSIONS 59

REFERENCES 61

1 INTRODUCTION

Molecular imaging is an emerging discipline in the field of biomedical research. Though already used routinely in diagnostics at clinical radiology departments; molecular imaging methods offer innovative non-invasive means, which in addition to diagnostics can be used to characterize and quantify biological processes at a cellular and subcellular level (Massoud & Gambhir 2003). In an experimental research setting this enables the longitudinal observation of intact living subjects with sufficient spatial and temporal resolution. Furthermore, the advances in multimodality imaging have introduced new methods to better understand biological responses through the use of molecular probes in addition to intrinsic sources of image contrast i.e. tissue (Willman et al 2008). A clear advantage over *in vitro* methods (e.g. cell cultures) is the use of intact living subjects. Furthermore, through the development of more sensitive devices, the use of small animals, such as mice or rats in addition to large animals, enable molecular imaging methods to be used in preclinical studies as well as in clinical studies.

Cellulose nanofibrils are nanometer range materials that are showing potential uses in many different fields of science, e.g. biomaterial studies (Klemm et al. 2011). The nature-based nanofibrillar cellulose (NFC) is from a sustainable source with unique characteristics. The nanoscale structure and dimensions enable many useful functions, which also however, present risks as the interaction properties become more dominant. In the literature review part, the main focus will be on the medical and life-science applications.

As a potential biomaterial, bacterial nanofibrillar cellulose (BNC) has already been studied extensively (Klemm et al. 2011). In addition, the properties of the material itself have been well characterized. However, the use of plant-derived NFC as a potential biomedical device has only been recently investigated (Borges et al. 2011; Mathew et al. 2012). Despite the similarities of the two materials, there are a few advantages and disadvantages with the use of wood pulp cellulose nanofibers. Mainly as the source of the material is nigh inexhaustible, it is easily sustainable for industrial scale production,

therefore being very cost efficient. However it has been shown that the shape and structure of bacterial nanofibrillar cellulose is more easily controlled, in addition to being more pure than the plant-derived NFC (Klemm et al. 2011). Therefore it is clear that the biocompatibility and other biomedical application research have been focusing more in the bacteria-synthesized material.

To evaluate the functionality of the nanofibrillar cellulose in *in vivo* conditions, the experimental part of this master's thesis focuses on a minimal invasive study of a plant-derived NFC to be used as a novel application, drug releasing hydrogel "implant". The release and distribution of three different compounds were investigated with a single-photon emission computed tomography and x-ray computed tomography multimodality device (SPECT/CT).

The other aspect of this master's thesis is to evaluate the plant-derived nanofibrillar implant as a potential biomedical device through the means of molecular imaging. Therefore the literature review part focuses mainly on SPECT/CT imaging and NFC, its characteristics in addition to current research and potential applications.

2 CELLULOSE NANOFIBERS

2.1 Properties

Cellulose is the most abundant naturally occurring biopolymer of glucose and it has been used for over 150 years as a chemical raw material in several fields of industry (Klemm et al. 2011). The structural features and reactivity has led to a creation of novel materials as well as advancements in composite materials, reinforcing existing properties (Pääkkö et al 2007). Currently applications for novel forms of celluloses are under investigation, namely the development of, and applications for nanoscale celluloses (Klemm et al. 2011).

The characterization and properties of nanoscale celluloses largely depends on the production method (Klemm et al. 2011). Top-down methods involve enzymatic, chemical and physical methodologies to isolate and separate individual microfibrils from plant cellulose, i.e. wood pulp (Fig 1). Microfibrils are bundles of cellulose macromolecule chains ranging from 5 to 60 nm in diameter and several micrometers in length. Another top-down method uses acid hydrolysis treatment to remove the amorphous sections from the microfibrils yielding in highly crystalline nanoscale cellulose rods or whiskers of 5-70 nm in diameter and 100-250 nm in length. Finally a biotechnological assembly method for nanofiber cellulose network synthesis is fermentation with sugars and plant carbohydrates in some bacteria (Klemm et al. 2011). The excreted film or gel is a stable and tight nanofiber network of fibrils 20 to 100 nm in diameter. However cellulose nanofibers synthesized by fermentation are pure (free of hemicelluloses), in addition, the plant derived products might have a small amount of biogenic residues such as lignin and pectin, thus requiring an additional purification protocol.

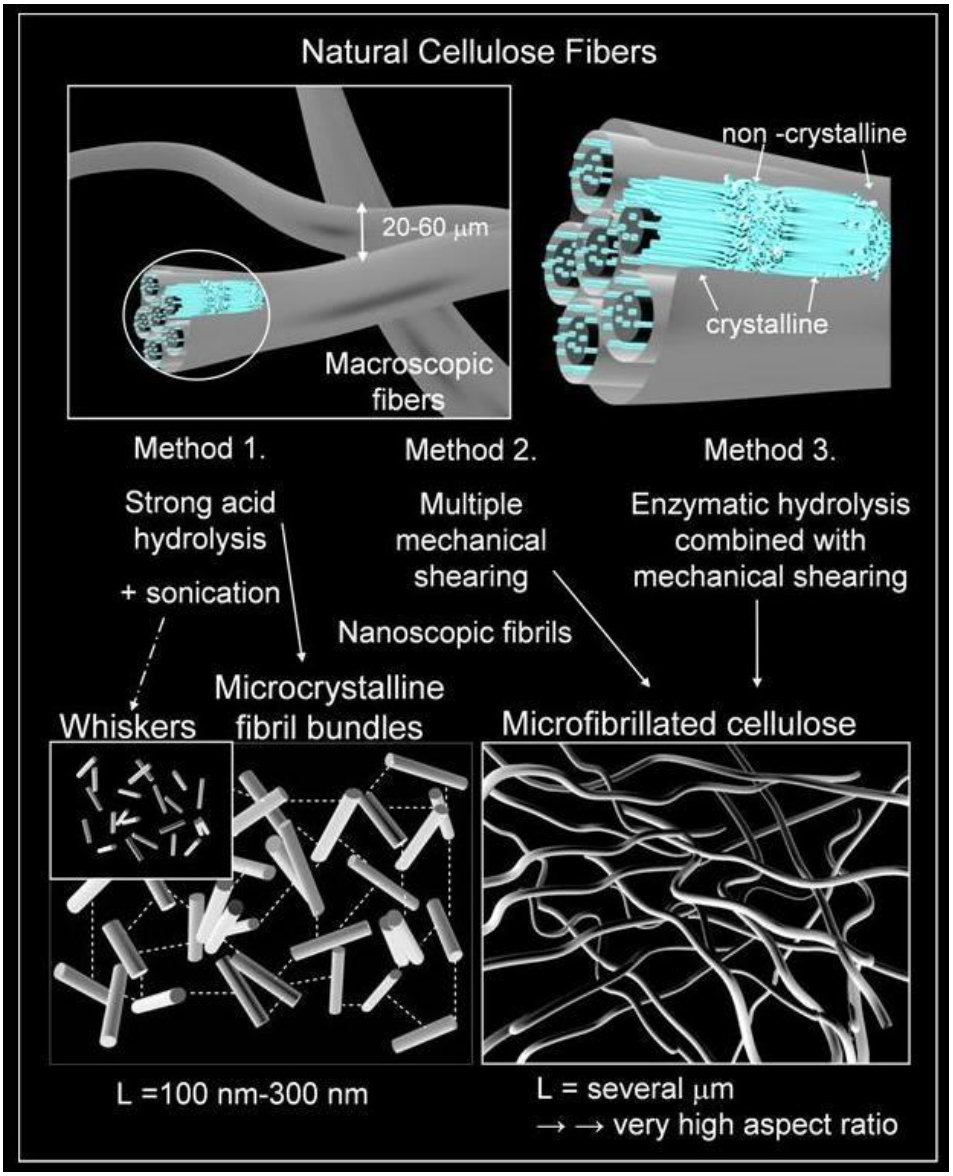

Figure 1. Schematics showing the release of cellulose nanofibrils from the natural fibers by different conversion methods. Different technologies yield in different products. Image taken from the Finnish Centre of Nanocellulosic technologies (VTT, Helsinki University of Technology, UPM).

The cellulose microfibril (or nanofiber depending on the nomenclature) aqueous suspensions behave as gels with pseudoplastic and thixotropic properties (Pääkkö et al 2007; Klemm et al. 2011). They are characterized by high water retention capabilities (i.e. gels are formed at very low concentrations), hydrophilicity and semicrystalline fiber morphology. Single fibrils have a very high stiffness rating (Young's modulus of 134 GPa) and tensile strength (2 GPa), with a small thermal expansion coefficient similar to glass (Klemm et al. 2006). In neutral pH, NFC is slightly negative in charge,

and the charge weakens as the surrounding pH is lowered (Kolakovic et al. 2012 B) In addition cellulose nanofibers have inherent versatile chemical modification properties (Eichhorn et al. 2001), which are important in producing additives and composites.

Cellulose microfibril dispersion storage modulus (the materials ability to store energy) and loss modulus (the materials ability to dissipate energy) are independent of angular frequency, in addition the storage modulus being high compared to loss modulus (Pääkkö et al. 2007), as it is with ideal gels. In contrast, classical viscous fluids storage and loss modulus are frequency dependent and the loss modulus is considerably lower than storage modulus (Klemm et al. 2011).

The storage modulus of microfibrillar cellulose is also highly dependent on the concentration and has a shear-thinning effect (Pääkkö et al. 2007), which is important in several industrial applications such as processing and coating (Klemm et al. 2011) The high modulus is due to the high strength of nanofibrillar network (Pääkkö et al. 2007). In addition highly controllable viscosity makes it versatile in its possible applications, as the modulus can be tuned 5 orders of magnitude by changing the concentration (Pääkkö et al. 2007). However shear-thinning has other benefits, for example in medicinal field or biomaterial research as it makes material handling much easier while retaining its desired viscosity in the application.

For further properties of NFC, there have been many studies investigating preparation methods, source materials and nanocomposite potential. In the review by Siró and Plackett (2010) these properties have been discussed in great detail.

2.2 Biomaterial research

Biomaterials are designed and constructed to interact with biological material, such as cells and tissue. Therefore they must be non-toxic, biocompatible, provide sufficient structural strength and properties as well as depending on the application either be biodegradable or non-biodegradable. Currently there are four different main categories of biomaterials: metals, ceramics, polymers and composites, each with their strengths

and limitations. However, nanoparticles and nanomaterials have unique physicochemical properties, which might cause an unexpected disruption of normal function in biological structures, as it is known that nanoparticles promote several different diseases and disabilities (Buzea et al. 2008).

Concern of cellulose nanofiber safety is related to its properties, such as needle like shape (rods, whiskers) and its persistence in body (i.e. non-biodegradable). However cellulose nanofiber structure is flexible unlike in inorganic fibres, which might alleviate the possible adverse effects from the needle like shape.

Studies of cellulose tissue biocompatibility have been made to investigate cellulose toxicity. The *in vivo* absorbance by living tissue seems to be dependent on the degree of crystallinity and the chemical structure; however reaction to foreign material in body was found relatively mild suggesting that cellulose is indeed biocompatible (Miyamoto et al. 1989). In another histological study on rats, a moderate foreign body tissue reaction was found (Märtson et al. 1999). However, 60 weeks after implantation, tissue recovery was observed and reaction to foreign material became milder. The subcutaneous implant did not degrade during the study period which indicates high biodurability.

Several studies afterwards have shown the safety of nanofibrillar cellulose. It was reported that no morphological changes were found, in addition to the absence of mRNA inhibition *in vitro* (Pitkänen et al. 2010). Nanofibrillar cellulose did not affect cellular growth or promote mutagenicity. Furthermore it has been shown that nanocrystalline cellulose does not cause genotoxicity (Vartiainen et al. 2011). Inflammatory effects and cytotoxicity have also been reported to be negative.

In biomaterial research it is important that the material acts as a template for a biomimetic purpose. Therefore it has to be biologically inert, i.e. non-toxic and biocompatible while still providing the desired functions for the application. Considering aforementioned nanofibrillar cellulose properties, NFC biomaterial could show usefulness as a connective tissue, replacement skin, bone composite or cartilage

material. In addition with the positive biocompatibility studies, nanofibrillar cellulose is a very promising material in the biomaterial research. However implant migration and non-biodegradability in living tissue might still be an issue in the future if not properly investigated.

2.3 Applications

Currently nanofibrillar cellulose is the subject of intensive research and development (Klemm et al. 2005). In addition, cellulose is a self-renewable raw material which makes it interesting for large industries as well. Cellulose biopolymers offer specific properties different from other natural and synthetic polymers, such as hydrophilicity, chirality, broad chemical modification capacity, semicrystalline morphologies and biodegradability depending on the application. These unique characteristics emphasize the bacterial and wood celluloses enormous potential in several applications on different fields of science.

The nanosized architecture and versatility of cellulose has tailored innovative products for science, medicine, food industry, paper industry and cosmetics (Klemm et al. 2006). Various types of celluloses are the design of controllable supramolecular structure in the production stage. The dominant source of cellulose is from plants, for example cotton in which cellulose is in near pure state. In addition non-pathogenic cellulose forming bacteria, namely *Acetobacter* strains, are suitable for cellulose production.

In nanoscale, nanofibrillar cellulose shows nanoporosity and transparency in dispersions and composite materials (Klemm et al. 2009). This is important in the fabrication of nanoporous membranes and scaffolds, for example in hard and soft tissue repair; basically mimicking a living system. In addition the chemical modification processes can be utilized through the carbohydrate-binding modules (CBM's; former cellulose-binding domain CBD; Gilkes et al. 1991). CBM's allow further modification of celluloses, for example in the formation of composites to strengthen material properties including biomimetic characteristics (Laaksonen et al. 2011). Additional ways of modification have been found through xylans (Linder & Gatenholm 2004), and utilized

in enhanced adhesion and proliferation of endothelial cells onto bacterial cellulose (Bodin et al. 2007).

The sustainability and vast sources of cellulose offer near unlimited and cost efficient raw materials for industry and science. Considering the biocompatibility and versatility, celluloses offer many new aspects in the development and design of several different and interesting applications in material sciences.

2.3.1 Bacterial cellulose

Bacterial cellulose has specific characteristics over nanofibrillar cellulose derived from wood pulp, which yields some unique properties mainly due to the biotechnological production technique (Klemm et al. 2005). Bacterial cellulose is a product of bottom-up method contrary to the plant derived top-down processing. Therefore bacterial cellulose offers different characteristics, such as the control of supramolecular structure and properties during cultivation, shaping of the material during biosynthesis, direct cellulose coating by thin layer cultivation, *in situ* composite formation, cellulose specificity, effective post process modification and very high purity (Klemm et al. 2009). Efficient ways to control the biosynthesis process (thickness, consistency, fibre network structure) include the choice of the bacterial strain in addition to the cultivation conditions, for example additional chemical additives. The shape can be controlled by different moulds and sintering techniques, most importantly the *in situ* production methods. This allows the formation of precise structures required for example in tissue grafts.

First applications of bacterial celluloses in the medical field were their use as wound dressings (Klemm et al. 2009). However in chronic wound healing bacterial cellulose has not shown significant effect as the persistent inflammation prevents normal wound healing processes (Wiegand et al. 2006). Therefore composite materials have been investigated and proposed regarding this issue, and the incorporation of collagen type I into the bacterial cellulose has shown to reduce degrading enzymes and pro-inflammatory interleukins (Wiegand et al. 2006). In addition, the properties of bacterial

cellulose have been assessed as a potential wet wound dressing application (Clasen et al. 2006) as it provides a moist environment resulting in better wound healing.

Another important factor in wound healing is to prevent microbial contamination. An antimicrobial effect has been achieved by impregnating and fixing silver nanoparticles inside the bacterial cellulose fibre network (Maneerung et al. 2007). Strong antimicrobial effect was shown against *Escherichia coli* and *Staphylococcus aureus*.

Furthermore, pellicular hydrogel like liquid films have been proposed for wound dressings and burn-healing (Jung & Jin 2007). In this study, another natural polymer formed by silk fibroin was introduced into bacterial cellulose to form a strong and flexible composite film in its wet state; a potential novel wound healing biomaterial.

However, other medical devices has been designed and proposed in addition to wound dressings. In biomaterials research nanofibrillar cellulose has been investigated as a possible use in orthopaedics (Hutchens et al 2006). In this study bacterial cellulose was combined with hydroxyapatite as a template graft for osseous defects. The biomaterial promoted bone colonization and degraded over time in replacement of new bone tissue. In addition, bacterial cellulose microvessels have been investigated for microsurgical implants, as in cardiovascular grafts (Schumann et al. 2009). Bacterial cellulose microvessels were implanted into defect carotid arteries in rats and pigs. The two studies show the bacterial cellulose vessel to be a potent, biocompatible and stable vascular conduit, which suggest it could be an approachable aspect in part of cardiovascular tissue-engineering programs. Additional *in vitro* studies on stress-strain responses of the carotid artery for tissue engineered bacterial cellulose blood vessels have been performed, showing similar properties than the porcine carotid artery (Bäckdahl et al. 2006).

Current research in bacterial cellulose consists of two main categories: wound dressings and novel active implants (Klemm et al. 2011). However, new designs have been proposed, such as bacterial cellulose scaffolds in cornea tissue engineering (Hui et al. 2009), and LiCl-impregnated bacterial cellulose, which shows bending actuation

properties in its hydrated state (Jeon et al. 2010). A possible application for a smart material where applying mechanical force will result in proportional ionic conductivity. Highly actuating and biocompatible material in a wet environment could be an interesting combination of properties in both sensor technologies and biomedical devices. Furthermore it has been shown that bacterial cellulose porosity can be controlled through density with different material handling processes (Hu & Catchmark, 2009), which is required in tissue engineering when an essential nanostructure is desired. In addition, a delivery method for targeted drug-delivery has been proposed with the use of ferromagnetism (Vitta & Thiruvengadam, 2012), which could be a potential application for targeted delivery of anticancer drugs.

2.3.2 Plant-derived cellulose

Plant-derived cellulose, or micro-/nanofibrillar cellulose, is obtained from wood pulp by applying mechanical pressure and grinding forces with chemical and/or enzymatic pre-treatment (Klemm et al. 2011). Proper delaminating processes require multiple passes through the homogenizers until a gel-like nanofibrillar ultra-structure is achieved. The energy consumption of the homogenization has been the main impediment of commercial production of nanofibrillar cellulose. However, after the discovery of using primary wall cellulose as opposed to secondary wall materials (Dinand et al. 1996), the production of nanofibrillar cellulose became more viable.

Plant-derived cellulose has been mainly used in technical applications (Klemm et al. 2011). Therefore wood pulp cellulose has already achieved great interest mostly in paper technologies and sciences (Ahola et al. 2008; Henriksson et al. 2008) as well as analytical purposes (Bonné et al. 2010). However, some studies have shown the potential benefit of plant-derived celluloses as biomedical applications and devices.

Native NFC hydrogels were studied and investigated as potential 3D cell culture scaffolds (Bhattacharya et al. 2012). The scaffolds were shown to provide feasible and biocompatible microenvironments for cell studies where the absence of other animal or human derived components is desirable. In addition, NFC hydrogel composites have

been investigated as potential replacements of the nucleus pulposus in regenerative medicine (Borges et al. 2011; Eyholzer et al 2011). The prepared hydrogels expressed biocompatibility with cartilage fetal cells (Eyholzer et al. 2011) and similar characteristics when compared with human nucleus pulposus, such as swelling ratios, compression moduli and viscoelastic behaviour (Borges et al. 2011). However, some differences were observed in the mechanical properties between the NFC hydrogel composites and the human nucleus pulposus.

NFC-polyurethane heart valves and vascular grafts have been shown to express good biological durability and haemodynamics (Cherian et al. 2011). In addition, good resistance against fatigue was observed in accelerated fatigue tests, where five out of five of the prepared heart valves exceeded the equivalent stress of 12 years cycle without failure. In addition to NFC-polyurethane grafts, collagen-NFC based implantable scaffolds have also shown to provide better mechanical strength and while retaining good biocompatibility (Mathew et al 2012 A). However, further optimization is required for a specific application; in addition to alternatives for problematic crosslinking agents which express cytotoxicity. Therefore, new compositions were grafted, referred to as "NF_{90}" and "NF_{120}" (Mathew et al 2012 B). Better cytocompatibility was achieved as well as a range of mechanical properties suitable for a potential artificial ligament or tendon application.

Plant-derived NFC has been studied as an enhanced stability and drug release matrix (Valo et al 2011; Kolakovic et al 2012 A; Kolakovic et al 2012 B). By limiting the rate of the drug release, a long-term sustained release application with good mechanical properties could be obtained. A steady sustained release was reported for up to 90 days in addition to almost zero-order release kinetics for two of the tree study compounds (Kolakovic et al 2012 B). For a system that requires a long-term sustained release, parenteral, topical and/or ocular deliveries were suggested as potential applications.

Furthermore, an oral application for controlling the postprandial concentrations of blood glucose, plasma insulin, glucose-dependent insulinotropic polypeptide and triglyceride was investigated (Shimotoyodome et al 2011). Therefore the administered TEMPO-

oxidized cellulose nanofibers were found to have potential in biomedical applications, such as to alleviate symptoms in the long-term complications related to patients with diabetes.

Generally it can be concluded that plant-derived NFC has potential use as an application in cell therapy and tissue engineering in addition to drug and chemical testing. These recent studies will most likely increase the attention towards wood pulp NFC in the biomedical field, in addition to the predominant bacterial NFC.

2.4 Future perspectives

The number of patents versus applications ratio for nanofibrillar cellulose is very high (Klemm et al. 2011), which indicates that the use of nanofibrillar cellulose as a new potential nanosized material is just in the beginning. The inherent colloidal and rheological properties along with the utility that comes with the high modification capacity will increase the interests in nanosciences towards NFC. The basic knowledge about the properties and safety of NFC has already been established; in addition the usefulness of BNC as a hydrogel has been demonstrated in numerous potential biomedical applications.

However the variety of possible applications of NFC is one of its greatest strengths. Mainly due to the modification properties and versatility as a composite material, many technical applications have been shown to improve existing technologies. In conclusion, the use of NFC as a renewable and cost efficient raw material in the constantly developing field of nanosciences will be a great asset to industry as well as towards nanotechnologies used in biomedical and other scientific fields in large variety. NFC is a valuable asset in the future especially as a nanoscale reinforcement material for further technological advancements, which will lead to a better quality of life of man as well as lessen the ecological burden by being environmentally safe and biodegradable. Simple and cost efficient production methods from an abundant and renewable source will also lower the economical hurdles of many costly industrial scale projects. The increasing attention will yield even more novel applications of NFC in the near future.

3 SPECT/CT

3.1 Single-photon emission computed tomography

Single-photon emission computed tomography (SPECT) is an imaging technique used in nuclear medicine. The working principle is similar to a conventional planar gamma camera; however the data acquired with SPECT can be processed into 3D images that are independent of patient position and orientation (Hirschmann et al. 2012). The 3D image datasets are constructed by a computer applying tomographic reconstruction algorithms to multiple projections taken from different angles with a gantry mounted rotating gamma camera (Fig 2). To hasten the image acquisition, multiple gamma cameras can be used simultaneously. Datasets are typically presented as cross-sectional slices through the patient; however these datasets can be freely manipulated as required.

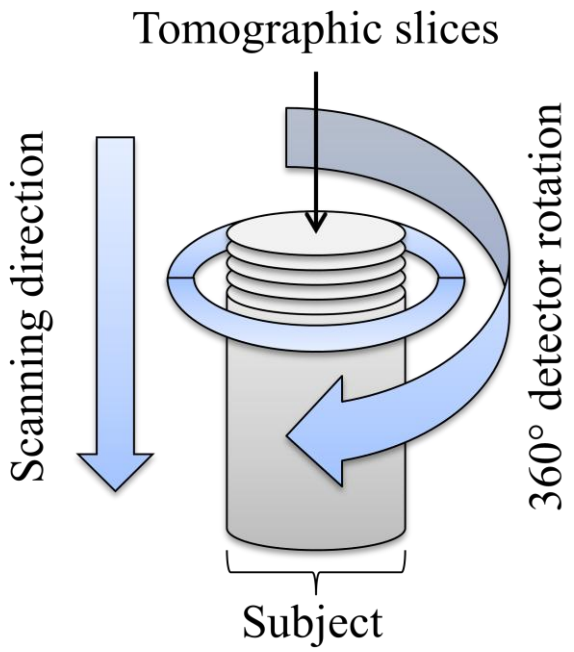

Figure 2. A schematic of SPECT acquiring projections during a scan. Detectors are mounted on a gantry which rotates around the subject (or patient) and detect the gamma energy emitted by radionuclides. Individual projections are reconstructed into tomographic slices that can be further reconstructed into 3-dimensional images. The reconstruction algorithms require time to process the raw data; therefore the full image can be acquired only after the full scan has been performed.

For its imaging purposes SPECT requires gamma-emitting radioisotopes (or radionuclides) that use ionizing radiation as a source of detection. A common detector system utilizes thallium-activated sodium iodide crystals (NaI(Tl)) to detect and convert the gamma ray energy emitted by the radionuclides (Fig 3). Energy is converted into visible scintillation light which is amplified by a set of photomultiplier tubes into electrical signals. This signal data can be readily reconstructed into tomographic images. Each radionuclide has its specific emission energy (keV); therefore it is possible to track multiple different radionuclides per scan if the main emission energies do not overlap with each other. In addition, with the current advances in nuclear physics, a number of radioisotopes with suitable half-lives can be produced readily with radionuclide generators or cyclotrons (i.e. particle accelerators) which can be utilized in numerous technologies, such as nuclear medicine. However due to the nature of gamma emission, a collimator is required to filter out scattering photons.

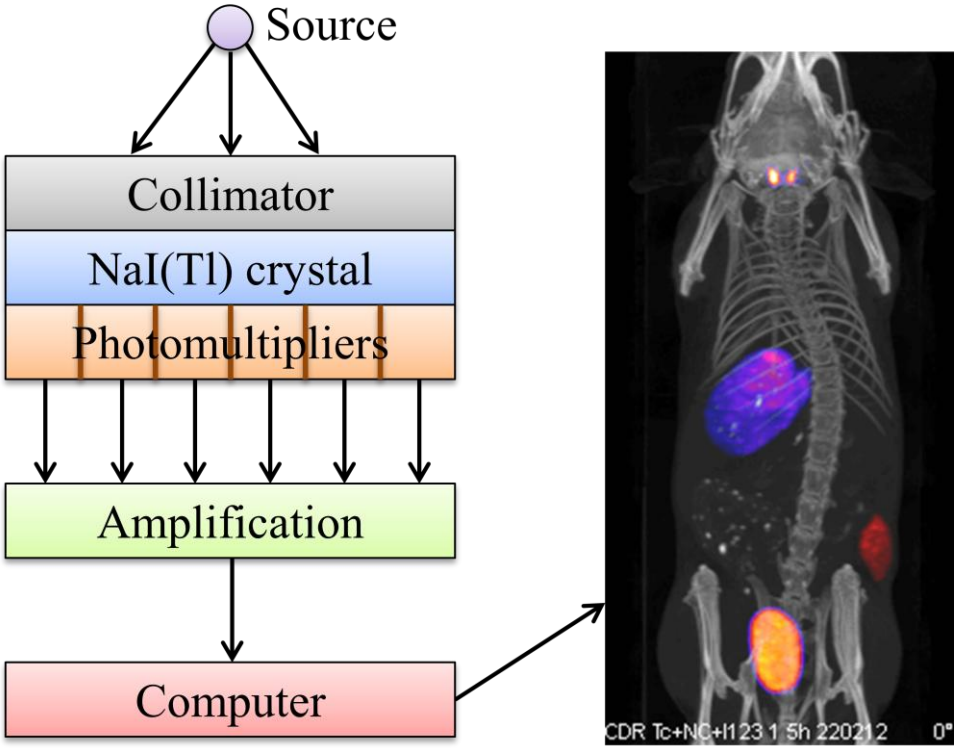

Figure 3. Gamma rays are detected by an inorganic scintillation crystal and converted into scintillation light. The signal is amplified and converted into electrical pulses that are recognized by computational softwares. A tomographic reconstruction algorithm assembles the projections into images.

Collimator is a lead plate with several holes in it. Lead absorbs photons which are not on a direct path to the detector (Fig 4). SPECT sensitivity and resolution is therefore determined by the number and diameter of the holes, in addition to the collimator thickness. Eliminating photons reduces SPECT sensitivity; however the resolution is improved yielding in much clearer images.

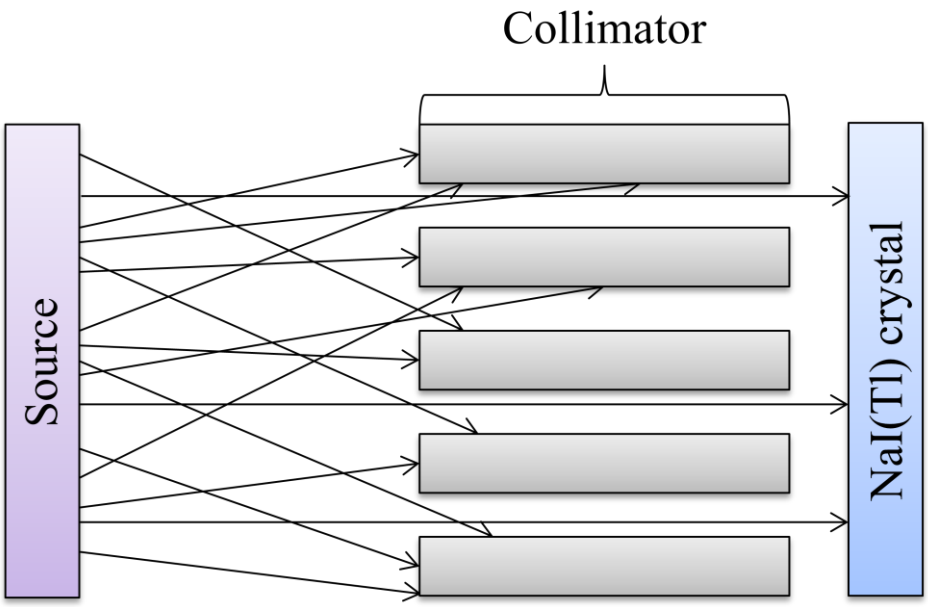

Figure 4. Lead collimators are required to filter out unfocused radiation from the source. Unparallel rays are not detected resulting in lower intensity and therefore sensitivity. Image resolution, however, will improve depending on the hole size, number of holes and collimator thickness. In principle, only the photons that are on a direct path to the detector will be detected.

Especially in small animal studies, different types of collimators are required to perform the image acquisition. Therefore new collimator designs are developed for greater sensitivity and image resolution (Rahmim & Zaidi 2008). Novel types of collimators are investigated to improve sensitivity without adversely affecting resolution.

3.2 Multimodality

In vivo imaging is an essential tool in gathering structural and functional data from a living subject non-invasively; however each imaging modality operates within a defined parameter space (Hasegawa et al. 1990). The parameter space is characterized by different factors such as spatial and temporal resolution, detection sensitivity, penetrating power and quantitative accuracy. Some modalities are well suited for certain applications while others are poorly suited for other applications; therefore combining different modalities into a single instrument can improve the imaging power of an application.

SPECT has a relatively low spatial resolution (Jaszczak, 1981), which can be improved by combining it with x-ray computed tomography (CT) (Hasegawa, 1990), which has an inherent high-contrast resolution. With CT it is possible to provide detailed structural information within tissue (especially bone) while the tissue functionality can be observed simultaneously with radioactive probes detected by SPECT; therefore combining the two aspects of different imaging modalities.

Multimodality enables the examination of function and structure in the same individual at the same time. In nuclear medicine this has led to more efforts in integrating other modalities into one device (Cherry, 2006). Most common systems have been introducing SPECT or positron emission tomography (PET) with CT. Other combination possibilities have been suggested and are commercially available, such as PET/MRI (Pichler et al. 2006) and SPECT/MRI (Goetz et al. 2008). Magnetic resonance imaging (MRI) presents some specific advantages over conventional CT, including high soft tissue contrast, absence of ionizing radiation and sensitivity to tissue alteration (Marzola et al. 2003). However several technical challenges delay the development of MRI multimodality devices (Cherry, 2009). Inherent high-power radiofrequency pulses that interfere with the scintillation detectors and electromagnetic waves generated by PET and SPECT power supplies and amplifier electronics makes it a difficult to combine these modalities. In addition to the moving parts of SPECT and

the need for a collimator are likely to create artifacts in the MR images, which further lag the development of a SPECT/MRI device.

In nuclear medicine SPECT/CT is now the standard application in cardiology in investigating coronary perfusion and myocardial viability, while it also has many applications in neurology and oncology (Rahmim & Zaidi, 2008). However some published results suggest PET/CT to be viable in certain cases where diaphragmatic attenuation is a hindrance factor (Di Carli & Hachamovitch 2006). In addition, due to fludeoxyglucose (^{18}F), or ^{18}F-FDG, PET/CT has been widely accepted in clinical facilities for diagnosis and monitoring of cancer.

3.3 Advantages & limitations

Due to the nature of SPECT systems the resolution is limited by technology and with the introduction of parallel-hole and multi-pinhole collimators the resolution and imaging speed has been greatly improved since the first single-pinhole collimators (Beekman & Vastenhouw, 2004). However this simultaneously lowers the sensitivity of the device, which can be somewhat overcome by lengthening scanning times. Technological limitation is an advantage over PET whereas its spatial resolution is always limited by physical factors (Rahmim & Zaidi, 2008). The intrinsic nature of positron type decay and PET coincidence detection system limit the theoretical achievable resolution at 2-3 mm, whereas 0.35 mm resolution has been achieved with current small-animal SPECT (Beekman & van der Have, 2007).

With PET the sensitivity is approximately two to three orders of magnitudes higher than with SPECT (Rahmim & Zaidi, 2008), as the coincidence detection system has no need for physical collimators. In addition, radionuclides with short half-lives can be injected in higher activities as the cumulative radiation dose remains the same as with emitters of longer half-lives. Higher activity administrations also improve signal to noise ratio and shorten scanning times, which makes it feasible to perform scans at different fields of view within reasonable time. However the longer half-life of single photon emitters

widens the detection time window allowing longer observation of the radioactive probes and therefore biological processes.

Attenuation correction is a challenge with both PET and SPECT (Rahmim & Zaidi, 2008). Photon attenuation is a property of emitted radiation interaction with materials (or tissue) as it passes through. This leads to a loss of detection due to absorption in the material or photons scattering out of the field of view. Attenuation increases image noise, artifacts and distortion; therefore attenuation correction for larger study subjects is required. Therefore patient differences and variety in tissue thickness further complicates the correction (Zaidi & Hasegawa, 2003). Mathematical algorithms applied in attenuation correction strategies are necessary for both PET and SPECT, with the exception of small animal imaging, where attenuation is not as significant due to thin tissue. Furthermore the integration of CT can be used to create attenuation maps for each individual subject during acquisition (Zaidi & Hasegawa, 2003). The internal anatomic structure provided by the X-ray computed tomography can therefore also be used for more precise attenuation corrections.

Time-of-flight (ToF) is the difference of arrival times of dual emitting photons; a feature that is used in modern PET imaging systems by detecting the times of arrival of the two 511 keV photons (Rahmim & Zaidi, 2008). With ToF it is possible to significantly improve image contrast versus noise (Karp et al. 2008), which is another sensitivity gain improvement. However in contrast to ToF, PET suffers from random coincidences, in which two annihilation photons are detected, but not originated from the same event (Rahmim & Zaidi, 2008). Random coincidence results in incorrect pair assignment and the annihilated photons true pairs remain undetected. Both ToF and the random coincidence complication are not present in SPECT.

Differences in single photon emitting radiotracer energies enable the dual-tracing approach for SPECT (Stodilka et al. 2006), which is impossible with current PET systems. Multiple energy windows can be monitored simultaneously with a single acquisition, which reduces acquisition times, image artifacts of a moving subject and subject discomfort (Rahmim & Zaidi, 2008). In addition different pharmacological

processes can be examined and different biological variables can be observed simultaneously e.g. drug pharmacokinetics. However, a crossover of multiple energy windows is present depending on the radiotracers used (Rahmim & Zaidi, 2008). The radiotracers energy windows might overlap resulting in one radiotracer contaminating the others energy window.

With specialized collimators (e.g. parallel and multi-pinhole collimators) it is possible to improve SPECT sensitivity without reducing image resolution (Rahmim & Zaidi, 2008). Therefore in future prospect, the sensitivity issues are lightened with the use of longer half-life radioprobes. In conclusion SPECT/CT offers good resolution and depth penetration for clinical and especially for pre-clinical imaging. To further improve sensitivity, and overall performance of the imaging modality; collimator technology, dual-tracing and attenuation correction still offer many challenges in the future. Furthermore PET/CT has received wide clinical acceptance due to the higher relative cost of SPECT/CT considering low fraction of its clinical indications (Rahmim & Zaidi, 2008). However pre-clinical use of SPECT/CT is viewed more cost efficient than PET/CT (Willmann et al. 2008). In general the imaging modalities are still considered more complementary than competitive.

3.4 Single photon-emitting radionuclides

Single-photon emission (or gamma radiation) is a form of electromagnetic radiation where the energy is emitted by unstable nuclei. The nucleus is in an unfavourable excited state and has to discharge some of its energy until it eventually relaxes to its ground state. The discharged energies can be detected by a gamma camera, which utilises single-photon emission. These emitters are called radionuclides or radioisotopes and when attached to another compound for the purpose of observing biological processes; radiopharmaceuticals, radioactive probes or radiotracers. The principle of introducing other compounds with radioisotopes was founded by a Hungarian chemist Georg von Hevesy in 1912.

3.4.1 Technetium-99m

Technetium-99m (^{99m}Tc) is a metastable decay product of molybdenum-99. It has a relatively short half-life of 6 hours and emits readily detectable 140 keV gamma rays and dissolves in water (Alberto et al 1998). ^{99m}Tc-labelled compounds are common in several medical applications; such as studying thyroid physiology and pathophysiology (Andros et al. 1965), childhood brain tumour diagnostics (O'Tuama et al. 1993), myocardial perfusion imaging (Wackers et al. 1989) and cardiac blood pool imaging (Thrall et al. 1978). ^{99m}Tc is ideal for medicinal use as it is relatively safe in terms of half-life and radiation energy. However the half-life is long enough, for example, to perform clinical and pre-clinical pharmacokinetics studies with drug molecules of similar half-lives. There are commercial kits available that provide the labelling protocols with several other pharmaceuticals. In addition water solubility enables ^{99m}Tc to be used intravenously as well.

3.4.2 Iodine-123

Iodine-123 (^{123}I) is a product of cyclotron proton irradiation where ultimately xenon-123 decays into ^{123}I (Fusco et al. 1972). ^{123}I has a half-life of 13 hours and decays mainly by electron capture which emits 159 keV gamma rays or to a lesser degree by internal conversion, emitting a low-energy Auger electron at 127 keV (Narra et al. 1992); therefore ^{123}I is not a pure gamma emitter, however the photon yield is high enough for the use with imaging systems (Fusco et al. 1972). In medical applications ^{123}I has been found useful in thyroid carcinoma diagnostics (Mandel et al. 2001), and as a labelled radiotracer in Parkinson's disease (Booij et al. 1998) and several different clinical dementias (Sharp et al. 1986).

3.4.3 Other radionuclides

In addition to ^{99m}Tc and ^{123}I several other radionuclides for SPECT are in medicinal use (Table 1). Radionuclides are used in consideration of their properties. However numerous studies are ongoing to improve the safety and efficiency of radionuclide use in general radiation work as well as current medical applications of SPECT and PET imaging (Cuaron et al. 2011).

Table 1. Common radionuclides used in SPECT medicinal imaging.

Radionuclide	Half-life (h)	Energy (keV)	Medical applications
Gallium-67 (^{67}Ga)	79.2	93, 184 and 300	Gallium-67 citrate; infections, granulomatous diseases and lymphoma diagnosis, temporal arteritis
Indium-111 (^{111}I)	67.0	171 and 245	In-111-DOTA-NAPamide; metastatic melanoma diagnosis In-111-DTPA; endocrine gastroenteropancreatic tumours
Iodine-123 (^{123}I)	13.3	159	I-123-Iomazenil; Benzodiazepine receptor binding, I-123-IMP; regional cerebral blood flow, I-123-β-CIT; dopamine transporter imaging (Parkinson's disease)
Iodine-125 (^{125}I)	1416	35	I-123-IACFT; dopamine transporter imaging
Technetium-99m (^{99m}Tc)	6.0	140	Tc-99m-MIBI; brain tumour diagnostics Tc-99m-HEXAMIBI; myocardial perfusion Tc-99m-HSA; cardiac blood pool imaging
Thallium-201 (^{201}Tl)	73	70 to 80	Tl-201; brain tumour imaging Tl-201; coronary artery disease diagnostics

3.5 Radiation safety

Ionizing radiation is not detectable by human senses; therefore the awareness of the dangers of radiation must arise from other sources, i.e. understanding the risks related to radiation work and knowing ways to protect oneself when handling radioactive material is important. In addition to this knowledge, recognizing any potential hazards and acting appropriately is the key principle in all radiation practices.

3.5.1 Regulatory issues

Due to the hazardous nature of ionizing radiation, the use of radioactive substances is guided by the radiation practices regulation. The regulation is based on the Radiation Act (592/91), which has been harmonized according to the basic safety standards laid down by the Council of the European Union in the Council Directive 96/29/Euratom. The nuclear safety and radiation practices regulations are issued by the Radiation and Nuclear Safety Authority (STUK, Finland), which belongs to the administration of the Ministry of Social Affairs and Health.

As a general principle, three main criteria must be met before the use of radiation and practices involving exposure is considered acceptable (Radiation Act, 2§). First in any task leading to possible exposure, the benefits must be greater than the detriment derived from the practice. Therefore one must always respect the justification of the purpose of the study; hence the principle of justification. Next the practice shall be arranged so that the hazardous health effects from exposure are kept as low as reasonably possible. As a principle of optimization, it is not enough that the maximum allowed exposure levels are not exceeded; an investigation must be made to explore all available methods to reduce levels of exposure as much as possible. Lastly according to the principle of limitation, no single person shall exceed the maximum prescribed values of radiation exposure.

In addition to the three principles, every instance using radiation must operate under a safety license (Radiation Act, 16§). License is granted by STUK when the applicant's organization and facilities meet all the requirements prescribed in the Radiation Act 2§ and that the necessary arrangements are made in the handling of radioactive waste and radiation sources.

Furthermore according to the Finnish Act on Animal Experimentation (62/2006) when animals are used for scientific purposes, all studies must be approved by the Finnish National Animal Experiment Board (ELLA) in addition to obtaining appropriate personal licenses in animal handling. The studies must also be in concordance with the

provisions laid down by the Animal Welfare Act (247/1996). The Ministry of Agriculture and Forestry is responsible for the implementation and enforcement of the Act's requirements.

3.5.2 Activity and exposure

The energy of ionizing radiation is measured in electron volts (eV), which is the energy of a single electron moving across an electric potential difference of one volt; therefore it can be calculated that 1 eV = 1.6 x 10^{-19} J. The energy of ionizing radiation is usually in between 10 keV – 10 meV.

The energy of radioactivity is usually related to radioactive decay. The speed of the decay of a radioactive material is described by the activity unit Becquerel (Bq). It determines the number of nuclear transitions during a period of one second; therefore the overall activity of radioactive material decreases over time as the number of radioactive atoms decrease due to nuclear transition. However the radioactive decay is also related to a decay constant (λ), which is characteristic to each radioisotope. Therefore the decay is exponential and enables the calculation of the half-life ($t_{1/2}$) of the radioisotope and a relationship between the parameters can be found: $\lambda = \ln 2 / t_{1/2}$.

Radiation exposure is measured in doses. Gray (Gy) is the unit for absorbed dose (D) which measures the amount of energy absorbed by a mass of one kilogram; therefore 1 Gy = 1 J / kg. The average absorbed dose per tissue or organ (D_T) can be calculated by dividing the amount of energy transferred from the ionizing radiation into the tissue by its mass: D_T = D / mass of tissue. The radiation detriment can therefore be estimated with two computational parameters: the equivalent dose (H_T) and the effective dose (E). The equivalent dose uses a weight coefficient (w_R) which varies depending on the type of radiation (Table 2). The equivalent dose values can be calculated when the radiation exposure is evenly distributed between the tissues and organs: $H_T = D_T \times w_R$.

The effective dose is used when a specific organ or tissue has been affected by radiation exposure or the exposure is unevenly distributed in the entire organism: $E = H_T \times w_T$. In

the effective dose the weigh coefficient (w_T) varies between tissue and organ types (Table 3). With the computational parameters, it is possible to assess the stochastic (probabilistic) effects of radiation exposure on the whole organism i.e. they are used to estimate the risks of long-term emerging detriments such as cancer or other genetic effects. However, ideal dosimetry is often difficult to estimate; therefore biologically relevant doses are studied through historical examples in hope to establish a standardized quantification of radiation exposure (Pass et al. 1997).

The unit for equivalent and effective dose is Sievert (Sv), which is also measured in amount of energy per weight (1 J / kg). However the unit gray is not interchangeable with Sievert as it is dependent on the biological context and or radiation type indicated by weigh coefficients; therefore Sievert is always used in the estimation of biological effects of radiation exposure.

Table 2. Weighting factors for equivalent dose calculations according to Euratom BSS and ICRP recommendations.

Radiation type	Radiation weighting factor w_R Euratom basic safety standards, 1996	Radiation weighting factor w_R ICRP recommendations, 2007
Photons	1	1
Electrons and myons	1	1
Neutrons < 10 keV	5	A continous function of neutron energy**
Neutrons > 10 - 100 keV	10	
Neutrons > 100 - 2000 keV	20	
Neutrons > 2 - 20 MeV	10	
Neutrons > 20 MeV	5	
Protons	5*	2
Alpha particles, fission fragments, heavy nuclei	20	20
* E > 2 MeV ** $2.5 + 18.2e^{-[\ln(E)]^2/6}$, E < 1 MeV ** $5.0 + 17.0e^{-[\ln(2E)]^2/6}$, E = 1 MeV - 50 MeV ** $2.5 + 3.25e^{-[\ln(0.04E)]^2/6}$, E > 50 MeV		

Table 3. Weighting factors for effective dose calculations according to Euratom BSS and ICRP recommendations.

Organ / tissue	Tissue weighting factor w_T Euratom basic safety standards, 1996	Tissue weighting factor w_T ICRP recommendations, 2007
Gonads	0.20	0.08
Colon	0.12	0.12
Bone marrow (red)	0.12	0.12
Lung	0.12	0.12
Stomach	0.12	0.12
Bladder	0.05	0.04
Chest/Breast	0.05	0.12
Liver	0.05	0.04
Thyroid gland	0.05	0.04
Oesophagus	0.05	0.04
Skin	0.01	0.01
Bone surface	0.01	0.01
Brain	0.05	0.01
Adrenals, small intestine, kidney, muscle, pancreas, spleen, thymus, uterus	0.05	0.12*
* Additional tissues included in the 2007 ICRP recommendations: extrathoraric region, gall bladder, heart, lymphatic nodes, oral mucosa, prostate		

3.5.3 Radiation detriment

The effects of radiation on tissue and cells are either somatic or genetic (UNSCEAR, 2006). Somatic detriments affect the exposed individual and genetic effects carry over to the next generation and therefore are hereditary. However, radiation is used to treat certain conditions e.g. killing cancer cells to reduce or eliminate cancerous tissue in radiation therapy.

Ionizing radiation causes cell death or prevents cell proliferation by damaging cellular DNA with inherent sensitivity to fast-replicating cells. Acute radiation syndrome (ARS) is a constellation of health effects caused by a loss of functionality in an organ or tissue when a sufficient amount of cells have died (Donelly et al. 2010). The onset of symptoms begins within 24 hours of exposure and may last several months (Table 4).

Table 4. Acute radiation syndrome symptom onset by dose of radiation exposure. Early symptoms are slight headaches, fatigue and weakness with mild leukopenia. Gradual increase of dose results in hemorrhage and infections, high fever, diarrhea, vomiting, nausea, shock, severe leukopenia and death. Until severe exposure of 6 gray and above ARS can still be treated with antibiotics, blood transfusions and stem cell transplants. At higher doses patients will receive mainly palliative treatment.

Dose (Gy)			
	≥ 12	Neurovascular syndrome onset	Multiple organ failure, certain death
	11		
	10		
	9		Severe leukopenia, probable death
	8		
	7		
	6	GI syndrome onset	LD50 with treatment
	5		Moderate leukopenia, LD50 without treatment
	4		
	3		
	2	Hematopoietic syndrome onset	~ 100 % survival without treatment
	≤ 1		

Somatic effects can be either deterministic or stochastic (UNSCEAR, 2006). Deterministic effects occur only when a certain threshold has been achieved. Exceeding the threshold always results in immediate appearance of symptoms specific to the tissue exposed to ionizing radiation. The occurrence of deterministic effects increase rapidly after the threshold is exceeded.

Stochastic effect occurrence is totally random and can be investigated only through statistical data (UNSCEAR, 2006). Stochastic effects are usually related to lower doses

of radiation exposure and therefore can be the result of a single normal cell mutating into a cancer cell. However the risks are low and it is difficult distinguish these effects from other sources that promote cancer. Risk assessments can still be done and an average risk of for example a malignant tumor growth or leukemia can be estimated.

3.6 Translational aspects

As imaging technologies mature, it becomes more apparent that the pre-clinical research protocols must have a direct translation to human applications. This requires fully quantitative and dynamic data gathering; therefore corrections for attenuation, scatter and especially partial volume averaging, as the latter is critical in imaging small structures of interest (Rowland & Cherry, 2008). In addition high-resolution detectors are necessary while still retaining an adequate sensitivity; however the main focus is how to translate the results from a mouse to man.

The sequencing of the mouse genome in 2002 introduced a key informational tool for understanding the connections between mouse and man (Mouse Genome Sequencing Consortium, 2002). Similarities in the genomes allowed the genetic engineering of mice strains, which could closely simulate human diseases. However, genetically engineered mice are highly priced and translational studies can easily induce prohibitive costs (Rowland & Cherry, 2008).

Ultimately small-animal imaging enables better understanding of mechanism of disease; in addition benefitting clinical practise. Improved disease detection, diagnosis and treatment response in clinical cases can be achieved with proper translation.

3.6.1 Clinical SPECT/CT

The clinical use of imaging units is mainly focused on oncological studies (Beyer et al. 2000; Mariani et al. 2010). Tumour detection, progression and response to treatment can be investigated with molecular imaging. Several different diagnosis methods already exist as well as increasing applications in minimal invasive surgery (Mariani et al.

2010). However, applications in several non-oncological diseases are also emerging. Diagnosis and prognosis of patients with cardiovascular diseases with SPECT/CT has been adopted in many medical units. In addition cell trafficking in stem cell therapy to understand stem cell-host interactions would be extremely difficult without *in vivo* imaging (Zhang & Wu, 2007).

The diagnostic accuracy of imaging units has ensured their usefulness in modern medicine, especially in tumour malignancy (Mariani et al. 2010). This has led to more extensive investigation of the possibilities of molecular imaging for non-invasive assessment of biological and biochemical processes in a living subject for clinical as well as in pre-clinical applications.

3.6.2 Small-animal SPECT/CT

Despite the connections between man and mouse genome, several challenges have to be addressed first to be able to understand and translate rodent data into human. Firstly the technical challenges; smaller objects need to be observed in great detail. Clinical imaging units do not have the sufficient spatial resolution to be able to gather satisfactory data (Rowland & Cherry, 2008). Therefore specialised units for small-animal imaging have been developed to overcome the limitations of clinical imaging; non-overlapping projections obtained with multi-pinhole collimation (McElroy et al. 2002) or coded aperture collimation where pinhole projections overlap the images onto the detectors (Schellingerhout et al. 2002).

Other specialised apparatus is required in small-animal imaging, such as an anaesthesia unit. Small animals, namely rodents, are difficult and time consuming to train to lie still (Rowland & Cherry, 2008). In addition, acquisition times can be lengthy; therefore the data is acquired while the animal is anesthetized. The state of consciousness affects the animal physiology and therefore might affect the kinetics of administered tracers. Some studies have been made to investigate the differences in tracer distribution between conscious state and anaesthesia and statistical differences have been found in brain and heart uptake (Toyama et al. 2004). To address this problem; attempts to validate the

physiological stability has been made to establish a reliable method to compare the kinetic results (Sharp et al. 2005).

For a small animal, the body surface area to weight ratio is much larger in comparison to a human, which leads to an effective heat loss. Therefore, bed warmers are necessary to maintain the correct body temperature while the animal is in anaesthesia (Hildebrandt et al. 2008). Not regulating the correct temperature might lead to different physiological activities that might interfere with tracer distribution.

To be able to administer radiopharmaceuticals to small animals, expertise as well as careful planning in animal handling and study design is required (European Union Council Directive 86/609/EEC). The route of administration might not be available for a rodent that would be used in humans; therefore alternative routes have to be used. In addition, all working (and sample) volumes are small, which have to be taken into account in the study planning e.g. is the equipment sensitive enough for analysis. In addition, differences in animal handling can affect study results (Fueger et al. 2006).

Dietary control might not be possible for small animals before acquisition. In some cases, food or water intake might affect the uniformity of multiple acquisitions (Hildebrandt et al. 2008). In addition it is unclear how the high radiation doses required in longitudinal studies affect these models, for example high doses could cause changes in tumour progression that might have an influence in the general response of the therapy (Rowland & Cherry, 2008).

Despite all the challenges involved in the translational aspects of small-animal imaging, it is clear that with new emerging technologies it is possible to achieve new clinical applications. Numerous advancements have been made, e.g. in cardiovascular molecular imaging; both SPECT/CT and PET/CT already have clinical use in the diagnosis and detection of several cardiovascular diseases (Buxton et al. 2011).

Recent subsequent breakthroughs in humanized animal models have also shown a great importance in studies of human cells, tissue and disease (Shultz et al 2007). Humanized

animal models are immunodeficient mice engrafted with human tissue, stem cells or peripheral-blood mononuclear cells. Therefore the study of human biological processes *in vivo* is possible without severe ethical and technical limitations. In humanized animal model studies, the immunodeficiency is first induced by sublethal irradiation of adult or newborn recipients, after which the haematopoietic system is repopulated with the use of self-renewing pluripotent human haematopoietic stem cells. Further advancements were made with the development of a complete functional human immune system, which provided the possibility to study both the innate and the adaptive immune systems *in vivo* (Traggiai et al. 2004).

Humanized animal models are important in the study of many infectious diseases that do not normally infect common laboratory species, e.g. AIDS or malaria (Shultz et al. 2007). In addition, humanized animal models can be used to study human autoimmunity, cancer and regenerative medicine. Especially in cancer and regenerative medicine, it is possible to utilize molecular imaging through immunodeficient strains that can be implanted with healthy or cancerous human cells without graft rejection. As SPECT/CT already has a firm foothold in tumour imaging (Keidar et al. 2003), in addition to recent studies in stem cell trafficking (Kraitchman et al. 2005). Therefore complementing the humanized animal studies with powerful analytical tools would likely to further benefit the research field in understanding human biological processes in cross-species environments.

3.7 Imaging as a tool for biopharmaceutical research

Molecular imaging has received increasing attention towards pre-clinical use, as pivotal trials involve considerable amount of time and significant costs (Willman et al. 2008). The increased investment rate of introducing novel drugs to the market subjects new strategies for evaluating promising drug candidates. With molecular imaging it is possible to observe biological activity, confirm drug targets and identify patients who would receive the most benefit. In addition, *in vivo* imaging allows the investigation of pharmacokinetics in an intact living organism; pharmacokinetic interactions (Guo et al. 2009), as well as biodistribution between and within tissues (Soundararajan et al. 2009).

The targeting and biodistribution of intended drug candidate can be examined when an imaging probe interacts directly with its target (Willman et al. 2008). In this approach, the endogenous expression of certain proteins can be used as targets (e.g. vascular endothelial growth factor receptor (VEGF) in a tumour). The labelled growth factor (e.g. ^{64}Cu-VEGF) can therefore be detected and quantified by its interaction with the receptor. In general, reporter genes that encode proteins that interact with imaging probes can be used. However, especially in the case of protein drugs, a proper delivery vector is required to introduce the imaging probe to into the tissue under examination. Therefore characterization of delivery vectors is required, e.g. siRNA delivery systems have already been successfully studied with molecular imaging in biopharmaceutical research (Merkel et al. 2009).

The strength of molecular imaging in pharmacokinetic studies lies within the possibility to observe intact living organisms as a whole, as it is near impossible to translate *in vitro* data to fully correlate with *in vivo* conditions. In addition, nuclear imaging allows isotopic substitutions of pharmaceuticals; the physiochemical characteristics of the radiopharmaceutical remain the same (Willman et al. 2008); therefore the imaging probe has the same properties as the parent molecule. However, it is possible to change the characteristics of the probe without careful design (bio-isosteric substitution; Willman et al. 2008).

Considering the conventional pre-clinical studies, with molecular imaging it is possible to retrieve more longitudinal data and statistical power using the same animal, also reducing the number of animals and cost. Furthermore the acquisition process is non-invasive and mostly automated. However, pharmacokinetic studies are largely dependent on the half-life of radionuclides, as tracking efficiency is reduced when the radionuclide half-life is shorter than the drug half-life. In addition, metabolism and protein interactions have to be taken into account. It is possible that the radiopharmaceutical is cleaved by a metabolizing enzyme so it becomes impossible to distinguish between the parent molecule and the metabolite. However molecular

imaging combined with intermittent plasma sampling can help to counter this problem, but will also increase cost and time.

Furthermore, it is possible to understand biological responses and therefore to assess treatment responses (Willman et al. 2008), e.g. dose dependency or toxicity. In addition molecular imaging has been used in compound screening (Kung et al. 2004). Therefore nuclear imaging is an attractive tool for drug development and especially in early pharmacokinetic studies, as many trials fail due to poor pharmacokinetic properties (DiMasi, 2001). Therefore, the role of molecular imaging is likely to increase in the near future of drug development and pharmaceutical studies.

4 AIMS OF THE STUDY

The aim of this study was to investigate the properties of plant-derived NFC as an injectable implant for drug release. In addition the diffusion characteristics and labelling properties of NFC were examined. The potential usefulness and safety of bacterial NFC in the medical field has already been established (Klemm et al. 2009). Furthermore only one study has previously suggested the use of wood pulp NFC as a potential medical device amongst other biomedical applications (Bhattacharya et al. 2012). However the differences and similarities between these materials have been comprehensively studied (Klemm et al. 2012), which allows the re-evaluation of the connections between the two nanofibrillar celluloses and further expand the possibilities of potential applications, for example in regards of biocompatibility and non-toxicity in biomedical sciences.

5 MATERIALS & METHODS

5.1 Diffusion study

NFC hydrogel was diluted to 1 % with ion free water. Fluorescein isothiocyanate–dextrans of 4, 20 and 70 kDa (Sigma-Aldrich, Finland) solutions were prepared respectively to the concentration of 125 µg/ml. Standard cell culture multi-well dishes with Ø 1.12 cm^2 well inserts were prepared for the diffusion study. In each well, 1 ml of ion free H_2O was added into the receiver compartment before the start of the experiment. 300 µl of 1 % NFC was pipetted on top of the well inserts, to the apical side, to form an even ~2.5 mm thick layer of hydrogel. 200 µl of each dextran solution in a total of 3 replicates were added on top of the hydrogel and the well plates were placed inside the incubator to maintain a constant 37°C temperature. At each time point the well inserts were shifted to a new well containing 1 ml of fresh ion free H_2O to simulate sink conditions. Well inserts were transferred to a new receiver compartment at 15 minute intervals for 2 hours and then at 150, 180, 240, 300 and 420 minutes. After the experiment samples were measured in a black 96-well plate (OptiPlate, PerkinElmer, Finland) with a multimode well plate reader Varioskan® Flash (Thermo Scientific, Finland), a fluorometric measurement with excitation and emission wavelengths 490 nm and 520 nm respectively. Permeability coefficient values were calculated from the first 5 time points for each dextran (P_{app} = dM/dt x 1 / (A x C_0), where P_{app} is the permeability coefficient, dM/dt is the efflux rate of the cumulative amount of study compound, A is the area of the well insert filter and C_0 is the initial solution concentration.

5.2 ^{99m}Tc-NFC labelling

^{99m}Tc-NFC was prepared with slight modifications according to the procedure described by Schade et al. 1991 for ^{99m}Tc-labelled carboxymethyl-cellulose. 1.6 % NFC stock (GrowDex™, UPM-Kymmene, Finland) was used to prepare 1 % NFC hydrogel with added stannous chloride stock (17.5 µg/ml in saline solution) and ^{99m}Tc-pertechnetate ($^{99m}TcO_4^-$) stock (~ 80 MBq/ml in saline solution) to a final volume

of 1 ml. Briefly, 590 µl of stock NFC was added to 285 µl of stannous chloride dehydrate solution (Angiocis, IBA Molecular, Belgium) followed with 10 minute incubation and mixing. Subsequently, 125 µl of $^{99m}TcO_4^-$ was added to reaction mixture to reach the NFC concentration of 1 % and incubated while mixing for 30 minutes.

The stability of the radiolabel was investigated in neutral isotonic pH by incubating the 1 % ^{99m}Tc-NFC samples for 24 hours. Samples were prepared in stock solutions as described above in saline or in fetal bovine serum (FBS) (Sigma-Aldrich, Finland). Radiochemical purity and efficiency was tested at every time point (0, 15, 60, 120, 240 minutes and 24 hours).

Labelling efficiency and radiochemical purity of ^{99m}TC-NFC was determined by TLC with ITLC-SG chromatography plates (Agilent Technologies, Santa Clara, CA, USA) in methylethylketone (MEK) solvent system. Plates were cut in smaller equally sized pieces and placed in standard RIA tubes for radioactive measurement with a gamma counter (RiaCalc. WIZ, Wallac 1480 WIZARD® 3'', Finland).

To optimize the method for ^{99m}Tc-NFC labelling, various conditions were tested during the labelling procedure, such as buffer pH ranging from 4.74 to 8.05, different incubation times for $^{99m}TcO_4^-$/NFC reaction mixture (5, 10, 15, 20, 25 and 30 minutes) and stannous chloride concentrations ranging from 50 to 0.05 µg/ml.

5.3 *In vivo* imaging

This study was approved by the Finnish National Animal Experiment Board and performed in accordance with the Animal Welfare Act (247/1996) and Good Laboratory Practices for Animal Research. The release properties of plant-derived NFC implants were investigated with the use of radiolabelled small compounds. Implants were injected subcutaneously in the pelvic region and the mice were observed non-invasively over a 24 hour period with the use of a SPECT/CT system. After the 24 hour period the mice were sacrificed by cervical dislocation.

A total of 20 BALB/c inbred mice were obtained from a professional stockbreeder (Harlan Laboratories, Netherlands) and quarantined for two weeks prior to the start of the experiment. The mice were divided into 7 groups, A, B, C, D, E, F (n=3) and G (n=2). The mice in groups A and C were injected with a mixture of saline solution and Iodine-123-Sodium Iodine (^{123}I-NaI) or a cocaine analogue Iodine-123-(2-beta-carbomethoxy-3-beta-(4-iodophenyl)-tropane) (^{123}I-β-CIT) (MAP Medical Technologies Oy, Finland) respectively. The mice in groups B and D were injected with a 5:1 mixture of 1 % NFC and ^{123}I-NaI or ^{123}I-β-CIT respectively (final mixture of 0.83 % NFC hydrogel with added study compound). Group E was injected with a mixture of ^{123}I-NaI and ^{99m}Tc-NFC for dual-radionuclide SPECT/CT. Groups F and G were injected similarly with 5:1 1 % NFC and ^{99m}Tc-labelled human serum albumin (HSA) (Sigma-Aldrich, Finland) or ^{99m}Tc-labelled HSA in a saline solution respectively (final mixture of 0.83 % NFC hydrogel with added study compound). All mice received 50-60 MBq/200 µl injections.

^{99m}Tc-HSA was prepared and radiochemical purity was tested according to the manufacturer's instructions (Vasculocis®, CIS bio international, France). Radiochemical impurities were found below the allowed 5 % of the total activity.

SPECT/CT imaging was performed with a four-headed small animal scanner (NanoSPECT/CT, Bioscan, USA), outfitted with 1.0 mm multipinhole apertures. All mice were sedated with isoflurane and SPECT images were acquired 0 h (with 5 or 6 acquisitions at 15 minute intervals), 5 h and 24 h post-injection in 16 projections using time per projection of 45, 90 and 180 seconds respectively. CT imaging was accomplished with 45 kVp tube voltage in 180 projections. For 3D co-registration and analysis the SPECT images were reconstructed with HiSPECT NG software (Scivis GmbH, Germany) and fused with CT datasets by using the molecular imaging suite InVivoScope™ (Bioscan Inc., USA). In the analysis, volumes of interests (VOI's) were drawn at the injection site (whole NFC implant), thyroid glands, stomach, left kidney, heart and around the striatum depending on the study compound respectively. Counts within each VOI were recorded, corrected for radioactive decay and normalized to the activity at the time of injection.

6 RESULTS

6.1 Diffusion study

From the study compounds the 4 kDa dextran expressed the fastest diffusion rate through the NFC hydrogel matrix followed by the 20 and 70 kDa compounds respectively (Fig 5). Relatively 100 % of the smallest dextran had diffused through at the 420 minute time point. 68.6 % and 58.1 % of the 20 and 70 kDa dextrans respectively were found at the receiver compartment at the end of the experiment, suggesting that the size is one factor contributing to the passive diffusion rate of dextrans through the NFC matrix. A decrease in the diffusion was observed in the beginning of the experiment for 20 and 70 kDa dextrans; however the cumulative amount of diffused 4 kDa is nearly linear. Later during the experiment the cumulative amount of diffused 20 and 70 kDa dextrans is nearly linear.

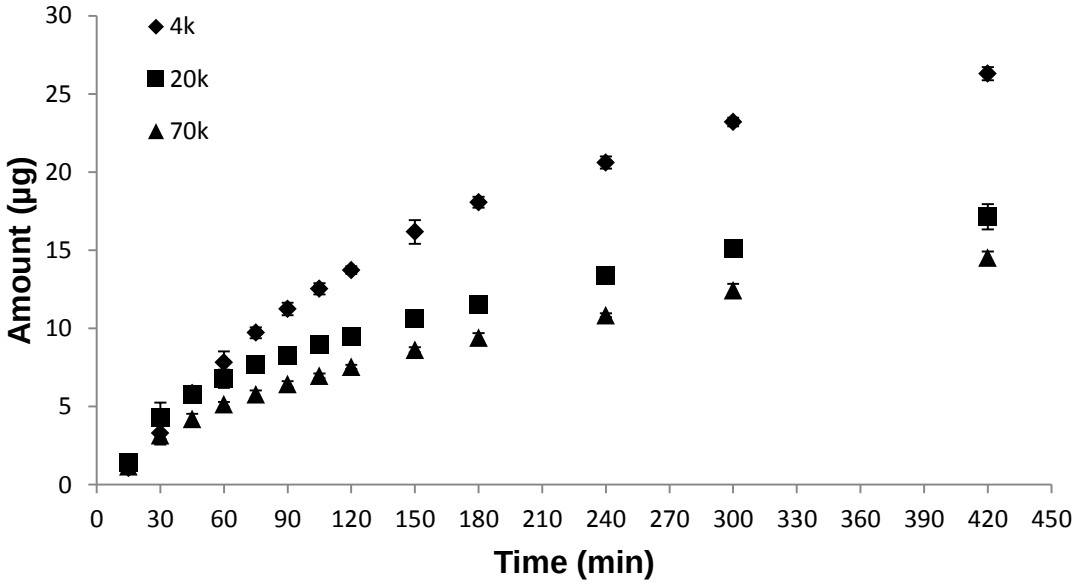

Figure 5. The diffusion of 4, 20 and 70 kDa dextrans through ~2.5 mm NFC hydrogel matrix. At the start of the experiment the diffusion rate of 4 kDa dextran is nearly linear suggesting that the NFC matrix does not hinder its movement. However the diffusion rate gradually decreases with the 20 and 70 kDa dextrans followed by a near linear diffusion later during the experiment, suggesting that the hydrogel layer is saturated first before the linear diffusion phase and the NFC matrix is hindering the movement of the larger compounds. 4 kDa dextran exhibits a slight decrease in diffusion rate at the end of the experiment as the amount of compound in the donor compartment is nearing 0 %.

The experimental Papp values for 4, 20 and 70 kDa dextrans were 8.75E-05, 6.01E-05 and 4.49E-05 cm/sec respectively (Fig 6). The permeation coefficient is nearly linear as the function of dextran size is on a logarithmic scale, suggesting that the molecular weight and size of the compound is a clear contributor to its diffusion rate through the NFC matrix. Therefore the limiting factor for the passive diffusion rate of dextrans is more likely physical and not a chemical interaction.

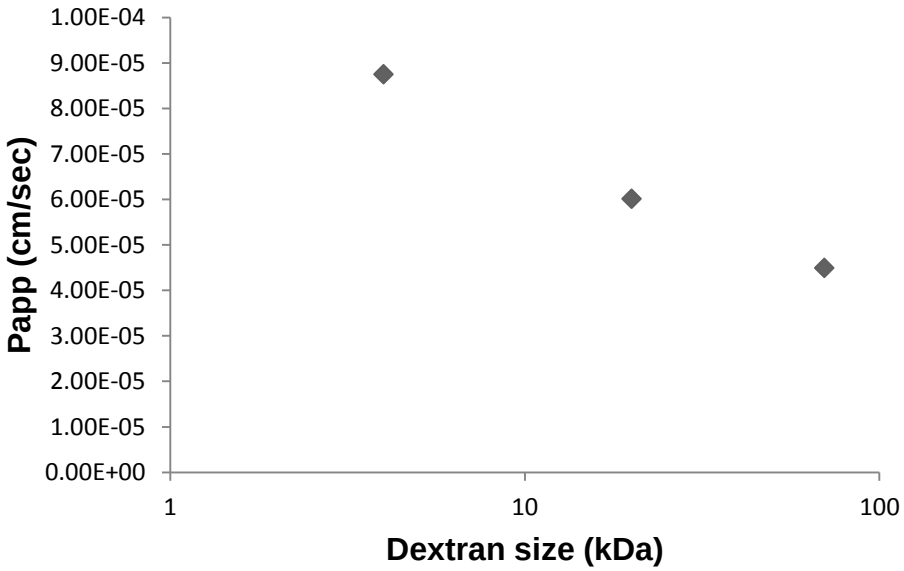

Figure 6. The permeability coefficient as the function of dextran size on a logarithmic scale. The experimental Papp values for 4, 20 and 70 kDa dextrans were 8.75E-05, 6.01E-05 and 4.49E-05 cm/sec respectively. The dextran size shows a linear behaviour towards the experimental Papp values. This suggests that the size of the dextran has a large contribution to its diffusion rate through the NFC matrix and the rate liming factor is physical and not chemical.

6.2 ^{99m}Tc-NFC labelling

The ^{99m}Tc-NFC labelling method was found highly efficient; typically resulting in over 95 % binding rate, while less than 5 % of the technetium remained unbound (Fig 7 & 8). Reference samples without stannous chloride showed little binding efficiency. In addition NFC did not show any inherent binding affinity towards ^{99m}Tc.

The amount of stannous chloride was investigated in the preparation of the radiolabel (Fig 9). It was shown that for the purpose of this experiment 5 µg/ml concentrations were the most optimal; however the labelling procedure was fairly insensitive towards the concentration changes of stannous chloride and no effect in labelling efficiency was found between the concentrations 50 and 0.5 µg/ml. 5 µg/ml was selected for further studies.

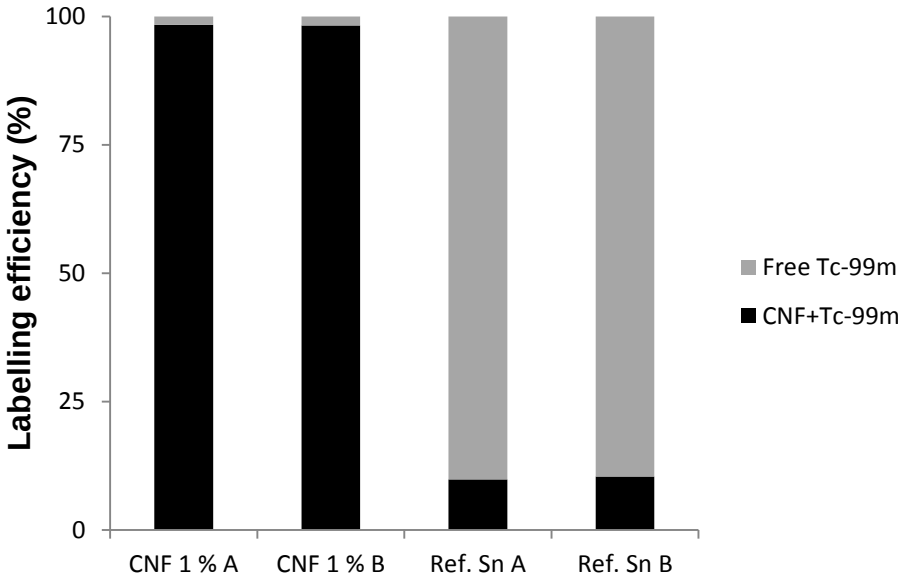

Figure 7. The labelling efficiency of ^{99m}Tc-NFC. Typically over 95 % binding was observed. NFC samples A and B were prepared with the aforementioned method, while reference samples A and B were not treated with stannous chloride. Samples that were not treated with stannous chloride showed poor labelling efficiency, suggesting that NFC does not have an inherent binding affinity towards the radiolabel in its unoxidized state.

The changes of pH in the dilution media was investigated during the radiolabel preparation. It was observed that the tested pH levels did not have any noticeable effect on the labelling efficiency (Fig 10). Throughout the pH range of 4.74 - 8.05, the labelling efficiency was found well over 95 %. The saline solution pH of 7.2 was selected for animal studies.

The incubation times before the TLC radiolabel purity confirmation were examined (Fig 11). From 5 to 25 minutes, the labelling efficiencies were ranging between 75.1 -

85.5 %. No clear cut off was found and the relative efficiencies between the incubation times did not show any major differences. However, it was shown that the incubation times less than 30 minutes were suboptimal. Therefore 30 minute incubation time was selected for further studies.

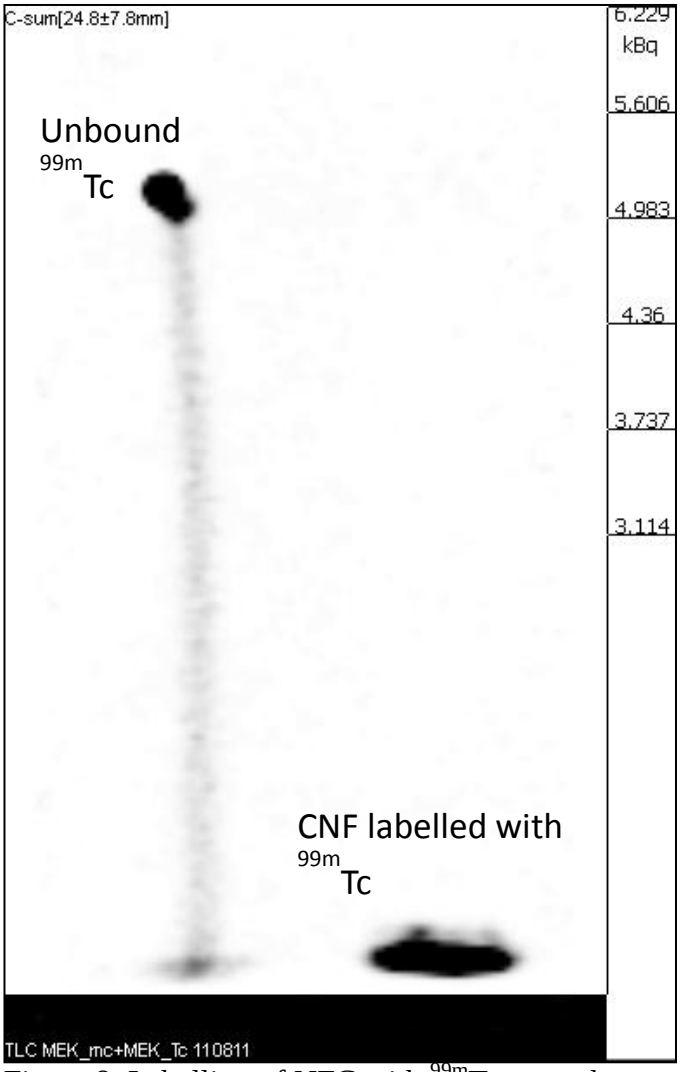

Figure 8. Labelling of NFC with ^{99m}Tc-pertechnetate. Left: with the absence of NFC the free $^{99m}TcO_4^-$ does not remain at the point of application. Right: NFC sample labelled with $^{99m}TcO_4^-$. Only a small portion of the radiolabel is shown unbound when mixed with NFC.

The radiolabel stability was studied in a period of 24 hours in both saline and fetal bovine serum (FBS) samples (Fig 12). ^{99m}Tc-NFC was shown to be stable during the 24 hour period while it was incubated in FBS. However, at the 24 h time point the

radiolabel functionality was lost in the saline sample (only 40.5 % labelling efficiency). During the first 4 hours the overall labelling efficiency remained at 81.7 and 87.2 % for saline and bovine serum samples respectively.

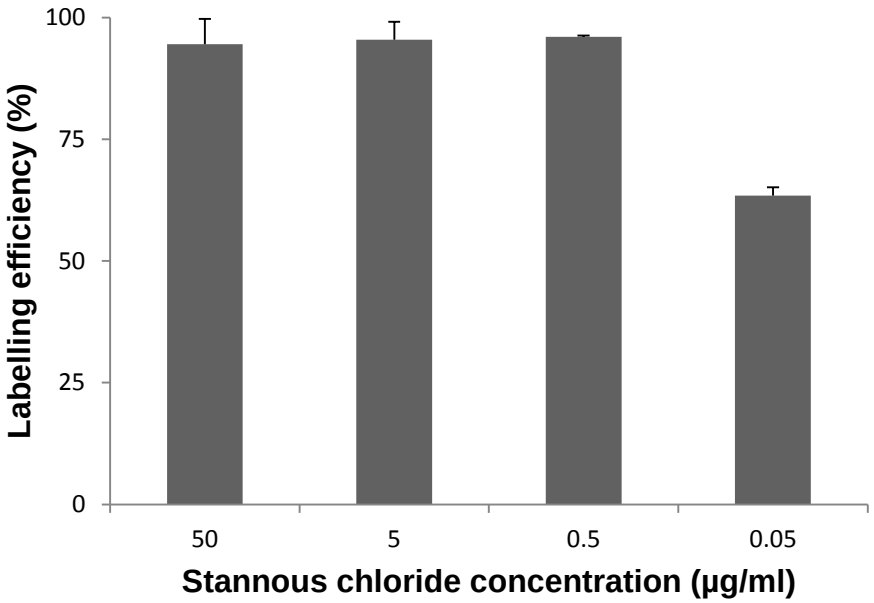

Figure 9. The effect of the amount of stannous chloride in the radiolabel preparation. No major differences were found between the concentration levels of 50 - 0.5 µg/ml of stannous chloride. 5 µg/ml was selected for the later phases of this study.

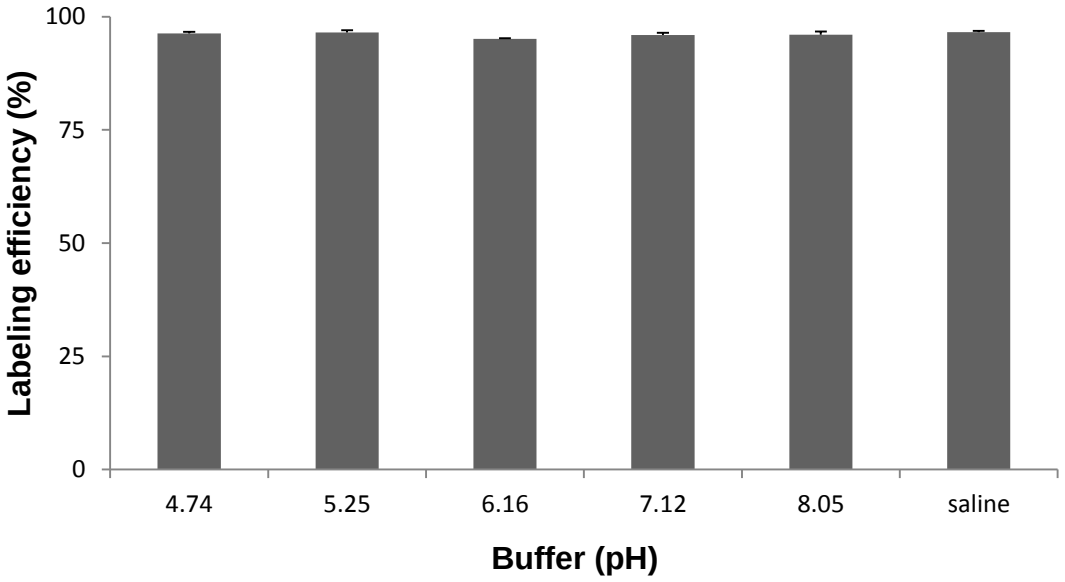

Figure 10. The effect of the pH level during radiolabel preparation. The sample dilution media pH levels between 4.74 and 8.05 did not show any clear effects in the final radiolabelling efficiency.

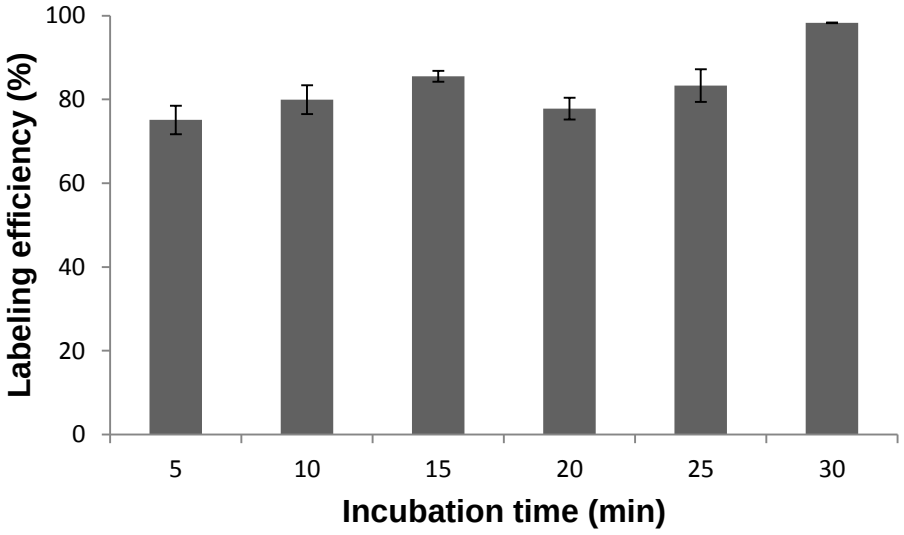

Figure 11. The effect of incubation times with stannous chloride before the ^{99m}Tc-NFC radiolabel is ready for use. Less than 30 minute incubation is suboptimal and over 95 % labelling efficiencies were not observed.

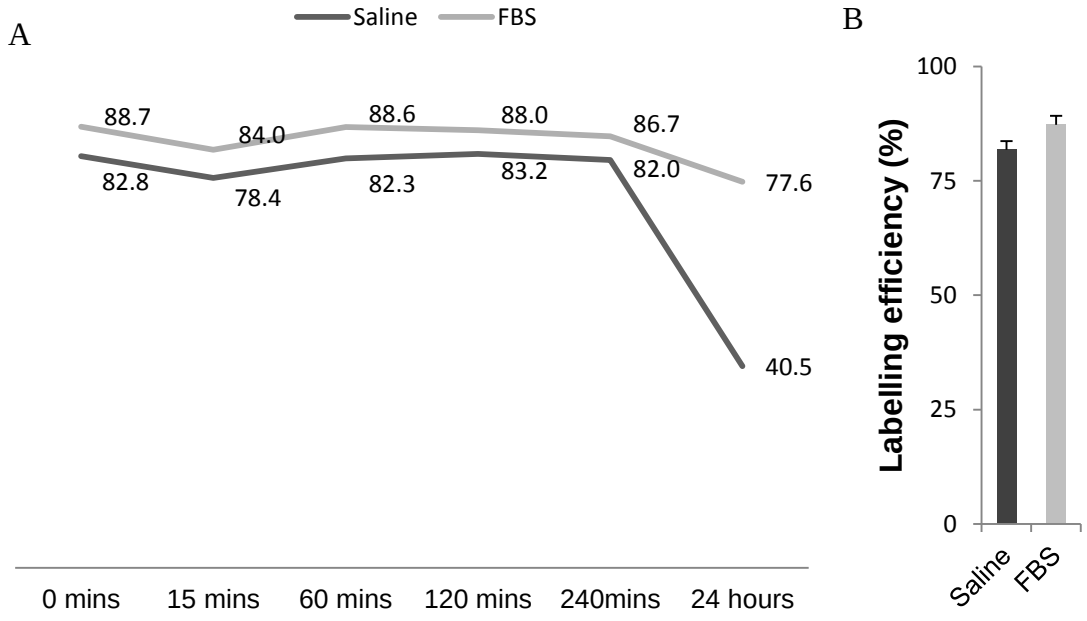

Figure 12. The stability of the ^{99m}Tc-NFC radiolabel during a 24 hour period. A) The sample prepared in FBS remained relatively stable during the whole experiment; however the sample prepared in saline showed a major decrease of labelling efficiency at the end point of the study. B) The overall labelling efficiencies suggest that both samples are highly stable during the first 4 hours after sample preparation.

6.3 *In vivo* imaging

The release and distribution of ^{123}I-NaI, ^{123}I-β-CIT and ^{99m}Tc-HSA was investigated after injecting the NFC implants imbedded with a study compound. In this preliminary study, compounds were selected to represent different sized molecules; two small molecule compounds and one large to verify the results from the diffusion study. Study compound and saline solution mixtures were used as controls. ^{123}I-β-CIT and ^{123}I-NaI were released rapidly from the NFC injections (Fig 13). 5 hours post injection both small compounds had been completely released from the NFC matrix. As a larger compound, ^{99m}Tc-HSA showed a slower release times from both NFC and saline mixtures. Furthermore, ^{99m}Tc-HSA expressed the slowest release from the NFC implants and 41 % of the injected dose remained within the implants 5 hours post injection. Fastest release profile was observed with ^{123}I-NaI, as half of the dose was already exited the biomaterial after the first time point, while around 30 % was released from the ^{123}I-β-CIT-NFC implants. A slightly slower release was observed with ^{123}I-β-CIT/NFC implants compared to the ^{123}I-β-CIT/saline injections; however for the two smaller compounds, the differences were not apparent regardless of the study compound or injection medium (saline or NFC). Differences between the HSA-NFC implants and saline injections were observed however. In addition, a large distribution of ^{99m}Tc-HSA was shown in the subcutaneous tissue surrounding the injection site indicating a very poor absorption of ^{99m}Tc-HSA into the circulatory system. Slight activity was detected within the bloodstream (heart and left kidney); however the distinctions between the compound itself and its metabolites can't be made, as it is well known that ^{99m}Tc-HSA does not pass the glomerular filtration under normal renal activity.

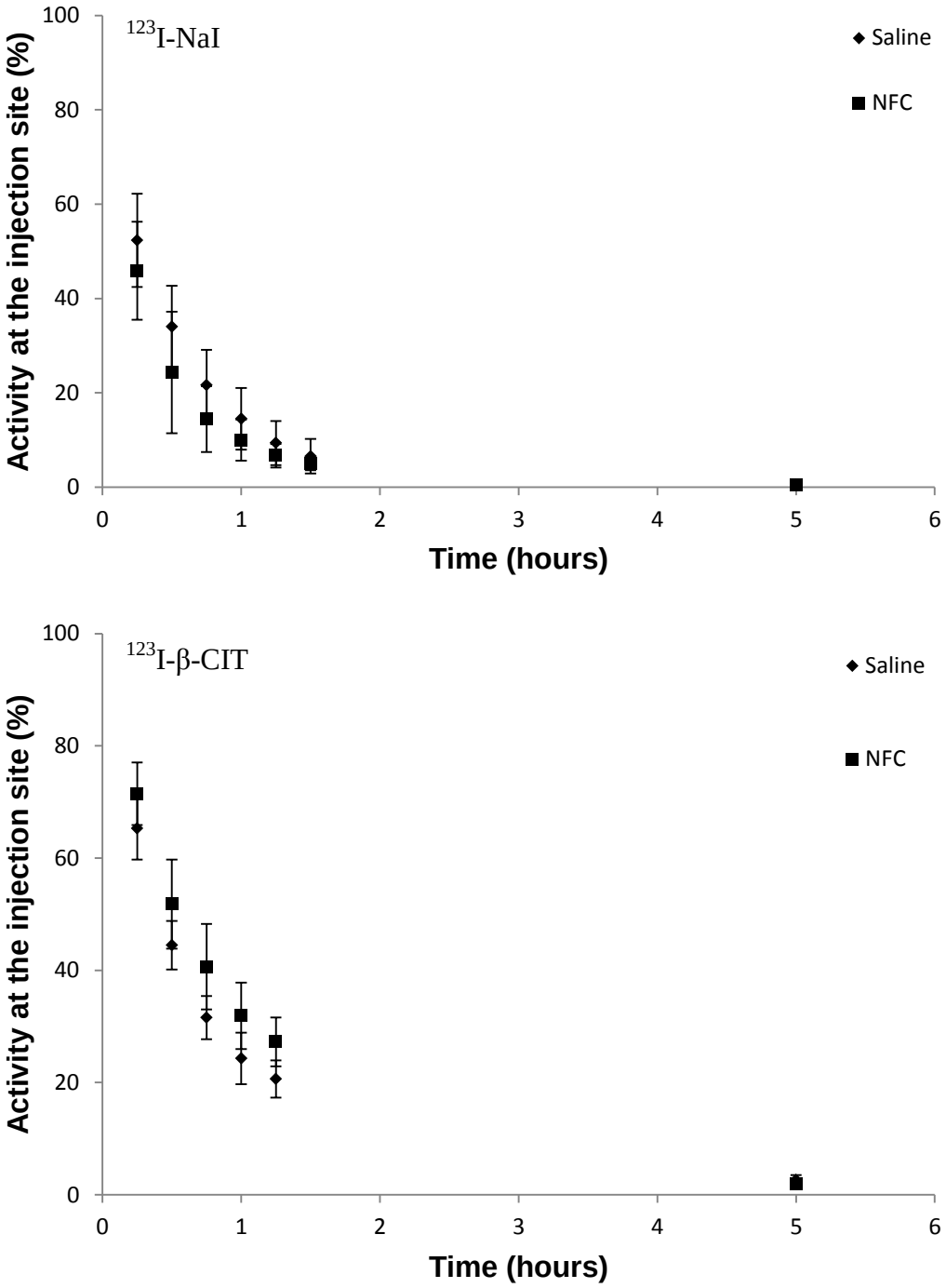

Figure 13. The release of ^{123}I-β-CIT and ^{123}I-NaI from NFC implants over a 5 hour study period (% of dose). Both compounds had been completely released from the implant 5 hours post injection. After the first time point, 50 % and 30 % of ^{123}I-NaI and ^{123}I-β-CIT had been released respectively. Faster release profile for ^{123}I-NaI was observed; however no major differences were found between the saline and NFC biomaterial injections for both study compounds.

^{123}I-NaI was mostly distributed into the thyroid glands and stomach, in addition to being excreted to urine (Fig 14). Saline and biomaterial injections showed similar distribution profiles in the stomach (Fig 15). However a delayed accumulation into the thyroid glands was observed with the ^{123}I-NaI-NFC injection (Fig 16). 5 hours post injection; no traces of study compound were found at the injection site (Fig 17).

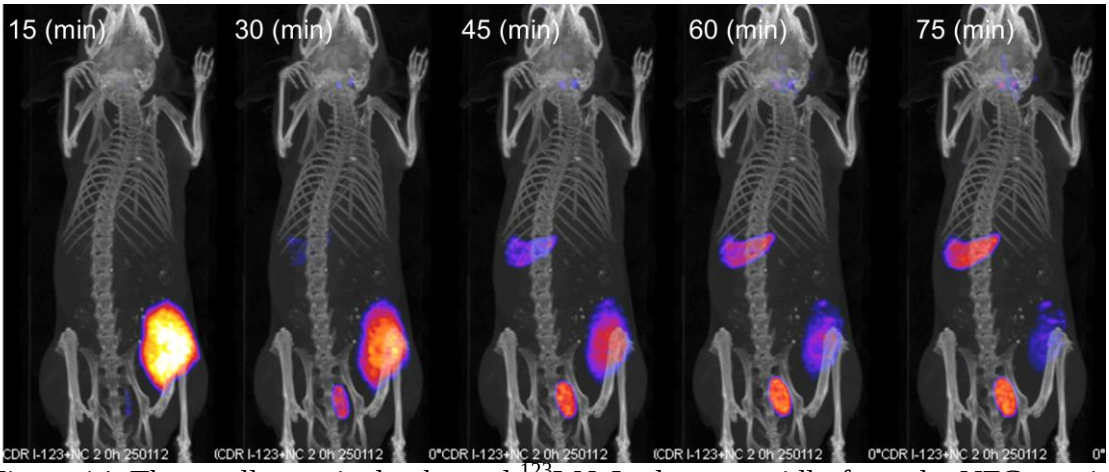

Figure 14. The small negatively charged ^{123}I-NaI releases rapidly from the NFC matrix. Accumulation was observed mainly in stomach and thyroid glands.

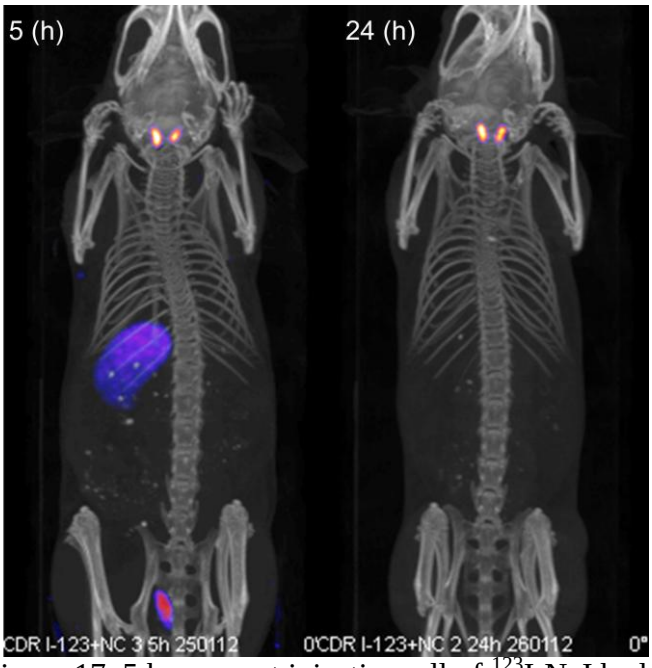

Figure 17. 5 hours post injection, all of ^{123}I-NaI had been released from the NFC matrix. 24 hours post injection, traces of study compound were found only from the thyroid glands.

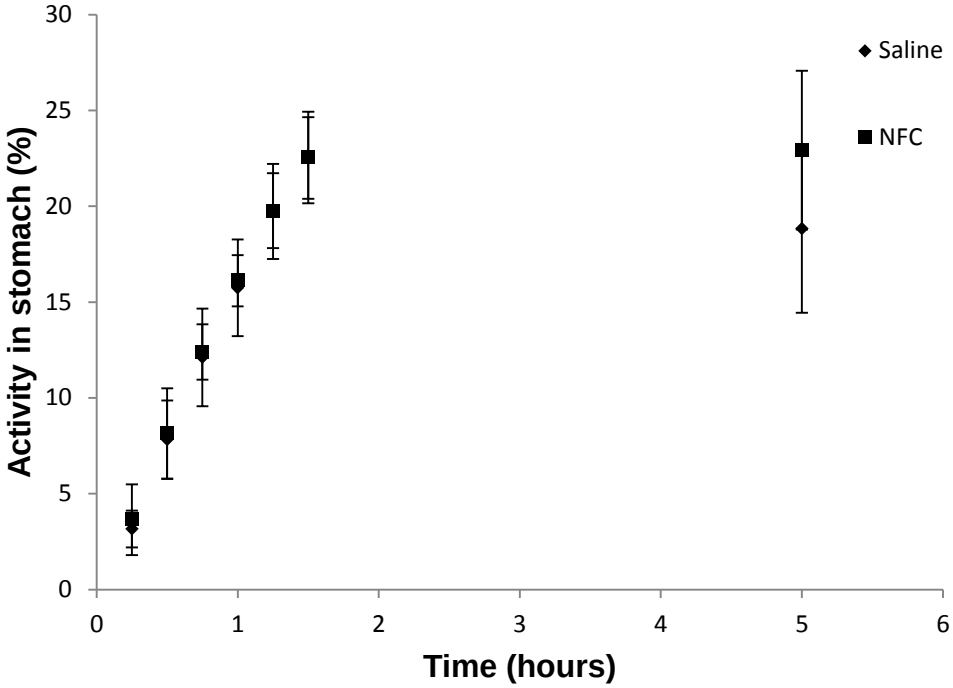

Figure 15. ^{123}I-NaI accumulation in stomach (% of dose). No differences were observed between the saline and NFC injections.

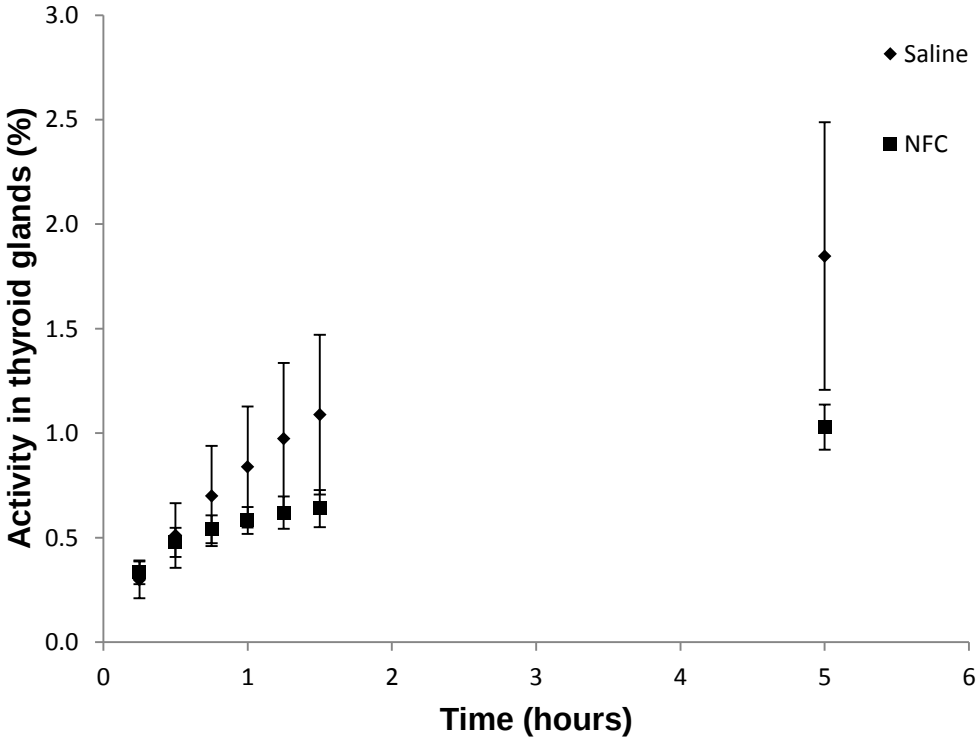

Figure 16. ^{123}I-NaI distribution into the thyroid glands (% of dose). A delayed accumulation of ^{123}I-NaI was observed when the study compound was injected with the biomaterial. However this contradicts with the results gathered from the injection site.

24 hours post injection 1.85 % and 1.31 % of ^{123}I-NaI dose was found in the thyroid glands for saline and NFC implants respectively. ^{123}I-β-CIT was mostly distributed into the striatum (Fig 18). Distribution into specific organs in the periphery was unclear and no other organs were selected. During the beginning of the experiment, a slight delay in distribution was observed with the ^{123}I-β-CIT/NFC injection compared to the saline injection; however the differences were not apparent (Fig 13). SPECT-CT images show that the study compound is more concentrated when administered with NFC, despite the similar release profiles (Fig 19).

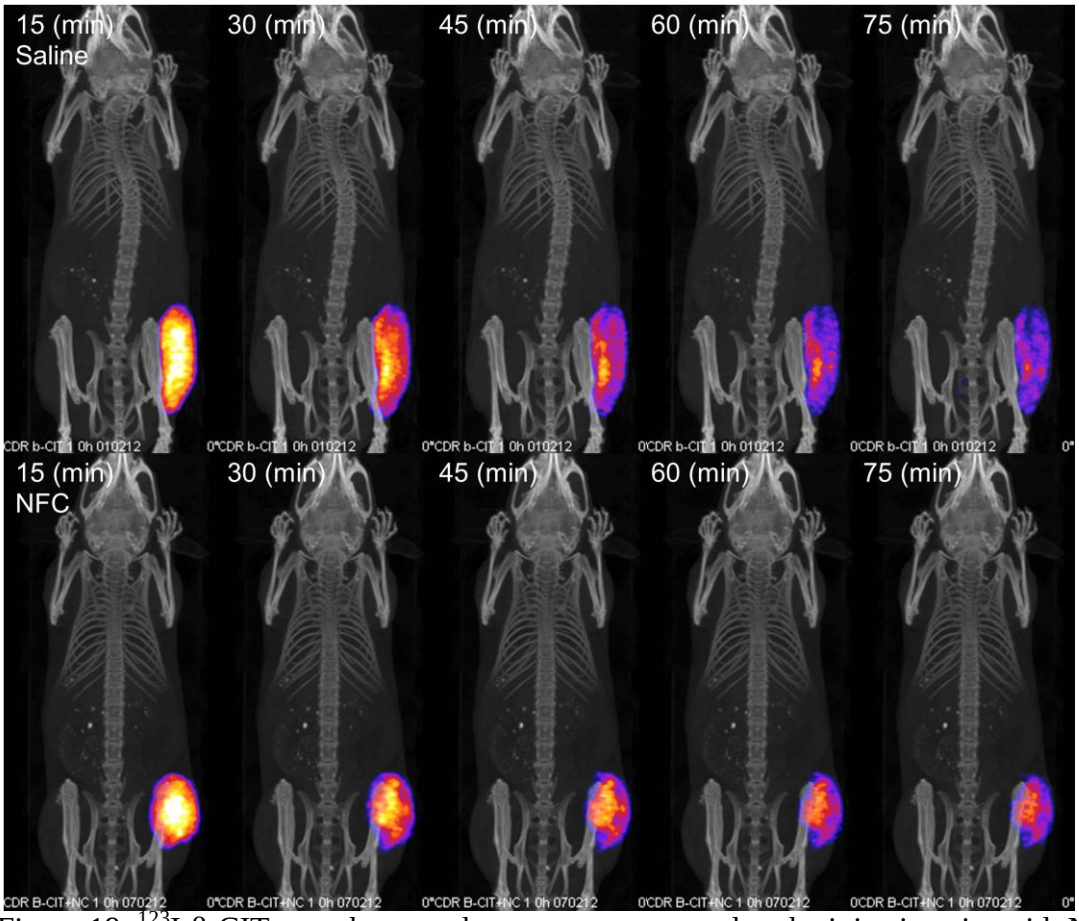

Figure 19. ^{123}I-β-CIT was shown to be more concentrated at the injection site with NFC injections. Saline injections distributed to a wider area inside the subcutaneous tissue. NFC retains the study compound to a smaller area; however the differences in rate of release/absorption were small between the injections.

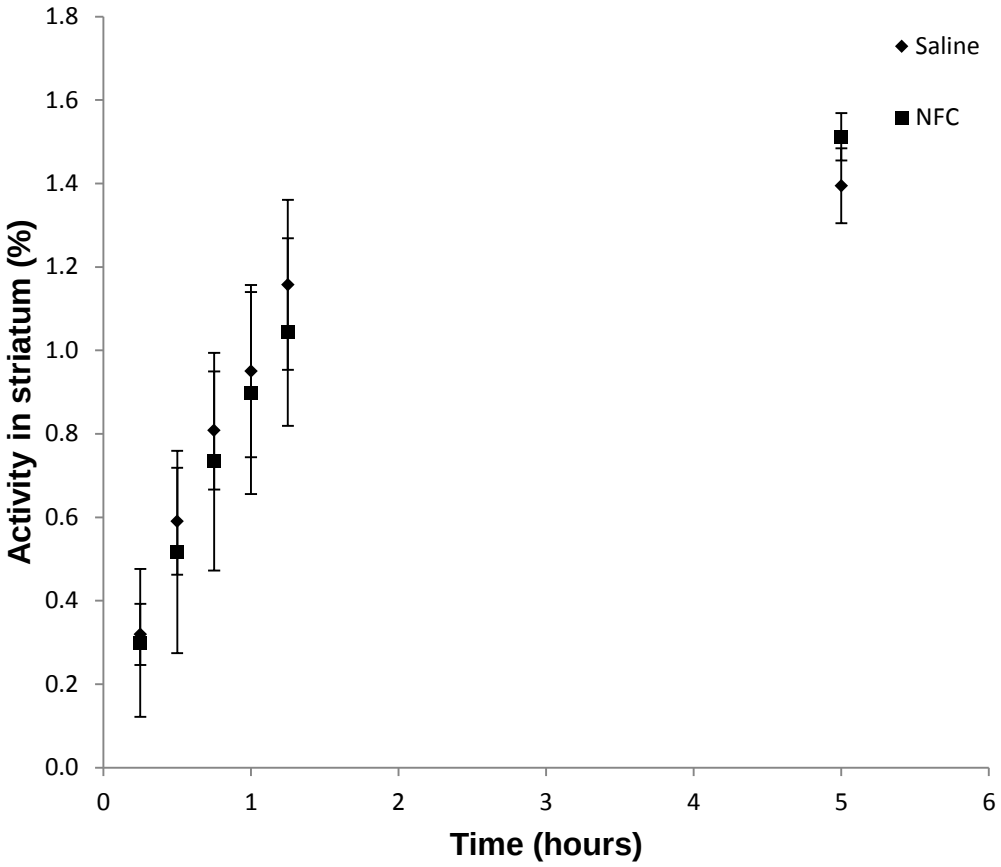

Figure 18. The distribution of ^{123}I-β-CIT into the striatum (% of dose). A slight delay in distribution was observed with the ^{123}I-β-CIT/NFC injections; however not apparent when compared to saline injections.

The distribution rate of ^{99m}Tc-HSA showed a clear difference between the NFC implant and saline solution (Fig 20). The release of ^{99m}Tc-HSA was steady during the 24 hour period. However, very poor absorption was observed and ^{99m}Tc-HSA distributed heavily in the subcutaneous tissue surrounding the injection site (Fig 21 & 22).

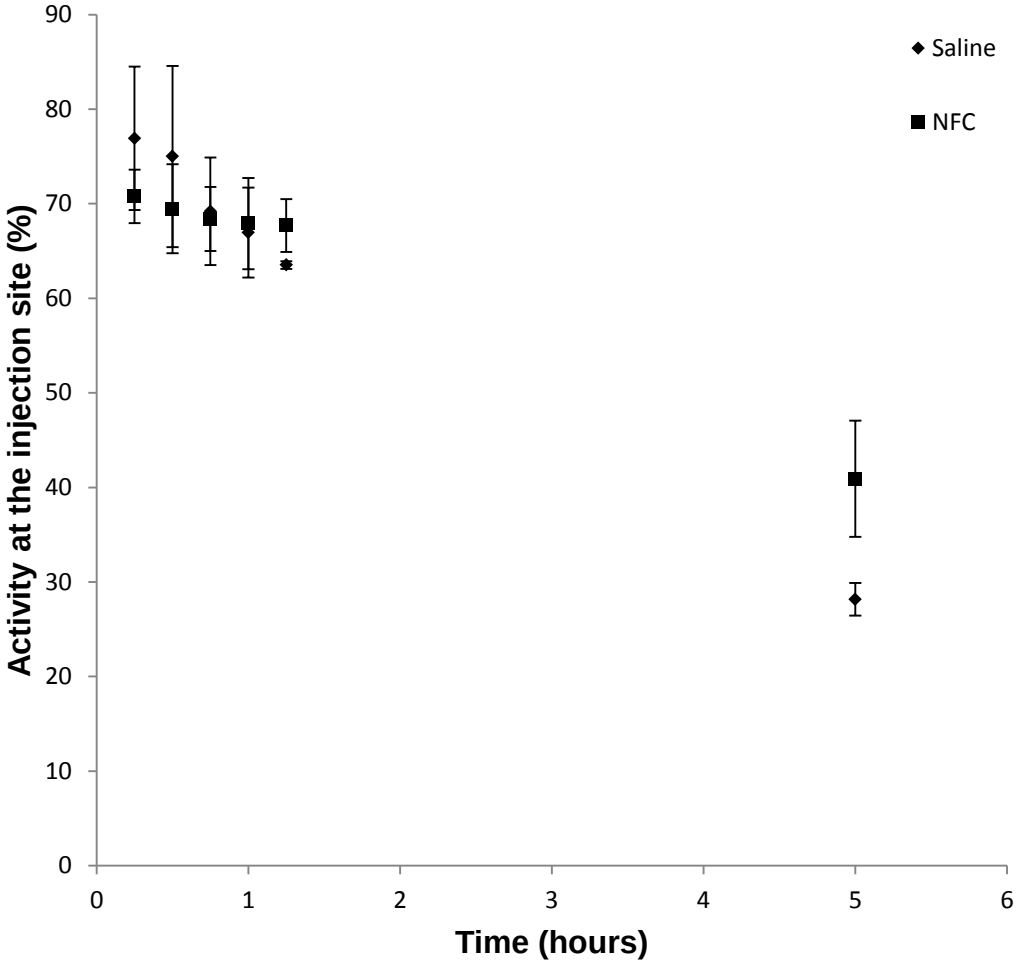

Figure 20. The release rate of ^{99m}Tc-HSA from saline and NFC injections over a 5 hour study period (% of dose). ^{99m}Tc-HSA showed a slower release profile than the smaller study compounds. In addition, a slower release from the NFC implants in comparison to the saline mixtures was observed. The release profiles for both saline and implant injections were steady.

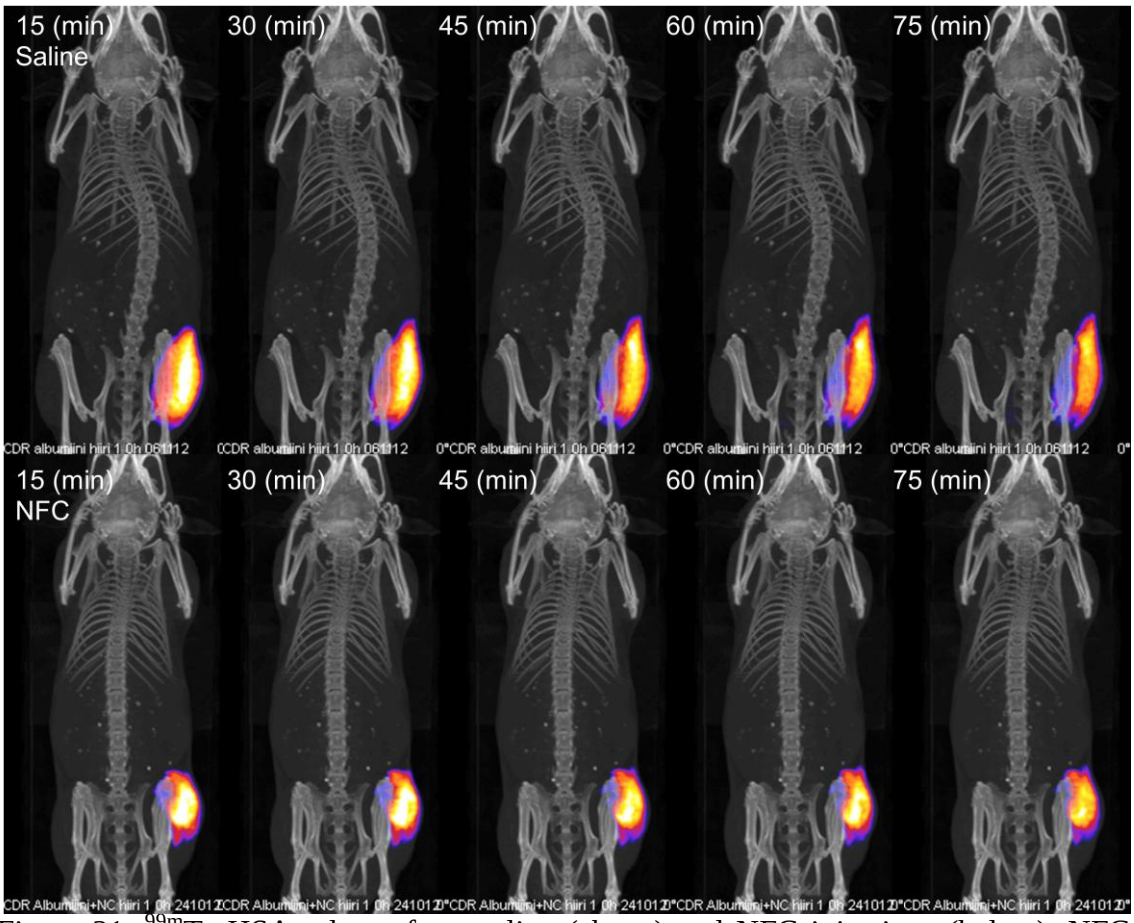

Figure 21. ^{99m}Tc-HSA release from saline (above) and NFC injections (below). NFC hinders the distribution of ^{99m}Tc-HSA within the subcutaneous tissue. In addition absorption is slow from both injections, probably due to the large size of the protein, and low enzymatic activity within the subcutaneous tissue.

Heart and the left kidney were selected to estimate the ^{99m}Tc-HSA absorption into the cardiovascular system. No apparent accumulation to any other organ for ^{99m}Tc-HSA was shown. No differences between the saline and implant injections were observed in blood pool activity, i.e. heart (Fig 23).

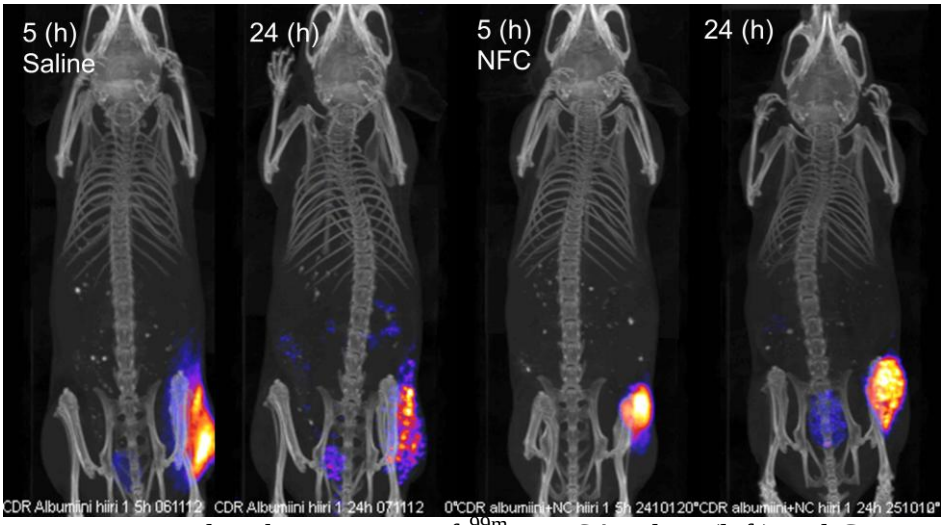

Figure 22. 5 and 24 hour images of ^{99m}Tc-HSA saline (left) and CNF injections (right). ^{99m}Tc-HSA is localized in around the NFC implants, and distribution in the subcutaneous tissue is much lower than in the saline injections.

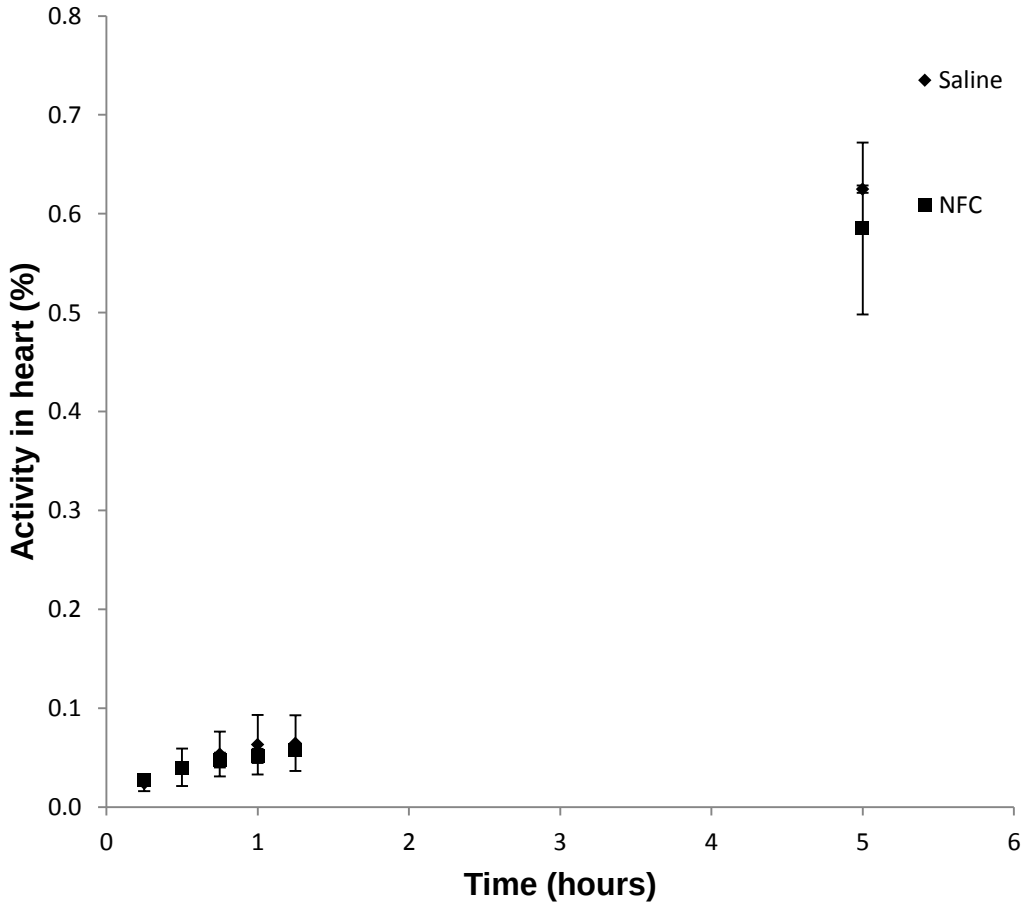

Figure 23. The blood pool imaging of ^{99m}Tc-HSA. Heart was used to estimate ^{99m}Tc-HSA absorption over the 5 hour study period. ^{99m}Tc-HSA expressed poor absorption from the injection site. No differences between the saline and implant injections were observed.

In addition to heart, the left kidney was observed to estimate ^{99m}Tc-HSA absorption (Fig 24). However, ^{99m}Tc-HSA should not easily pass through the glomerular filtration; therefore the left kidney is a better representative of its metabolites.

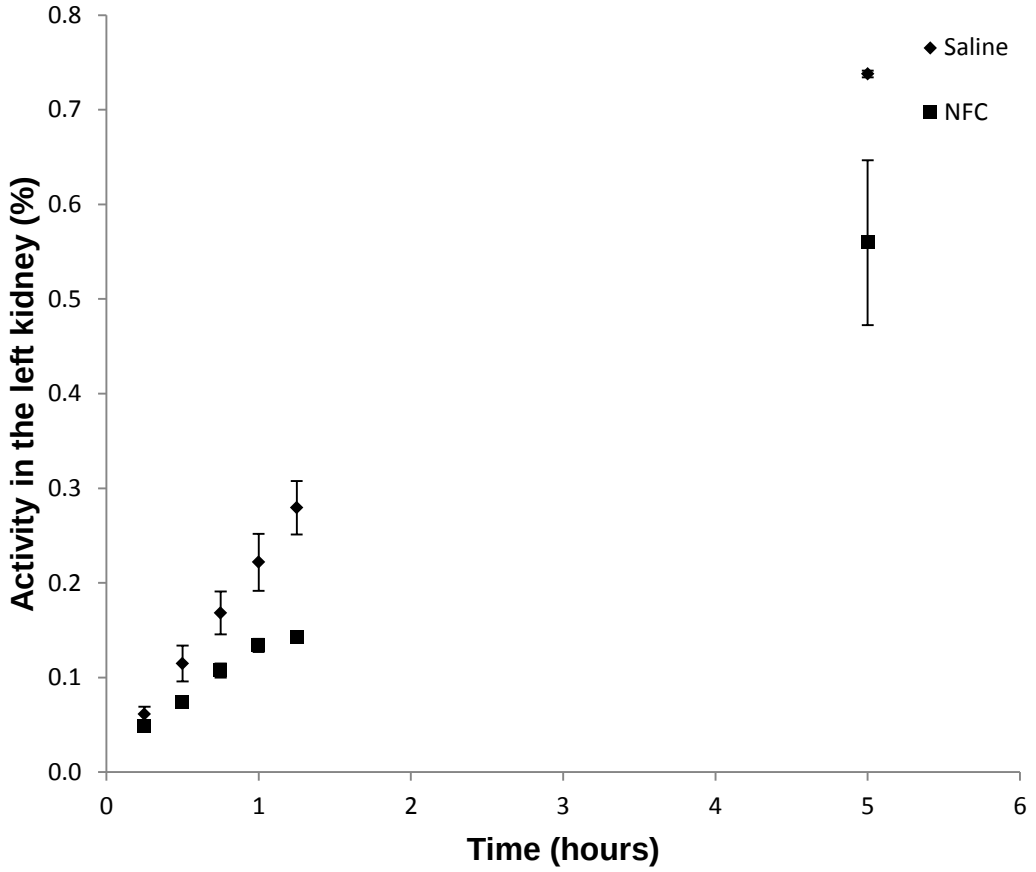

Figure 24. The accumulation of technetium in the left kidney over a 5 hour study period. The amount observed was low for both saline and implant injections. The activity in the left kidney is most likely due to metabolized ^{99m}Tc-HSA.

The dual-tracing experiment was carried out with ^{99m}Tc labelled NFC and imbedded with ^{123}I-NaI. SPECT/CT images confirm the implant position in the pelvic region post injection (Fig 25 & 26); in addition the implant has remained intact during the whole experiment. The mice were awake and moving between the acquisitions. During this time the implant has not migrated nor disintegrated. Furthermore the radiolabel showed stability and the pertechnetate remained at the injection site within the NFC implant.

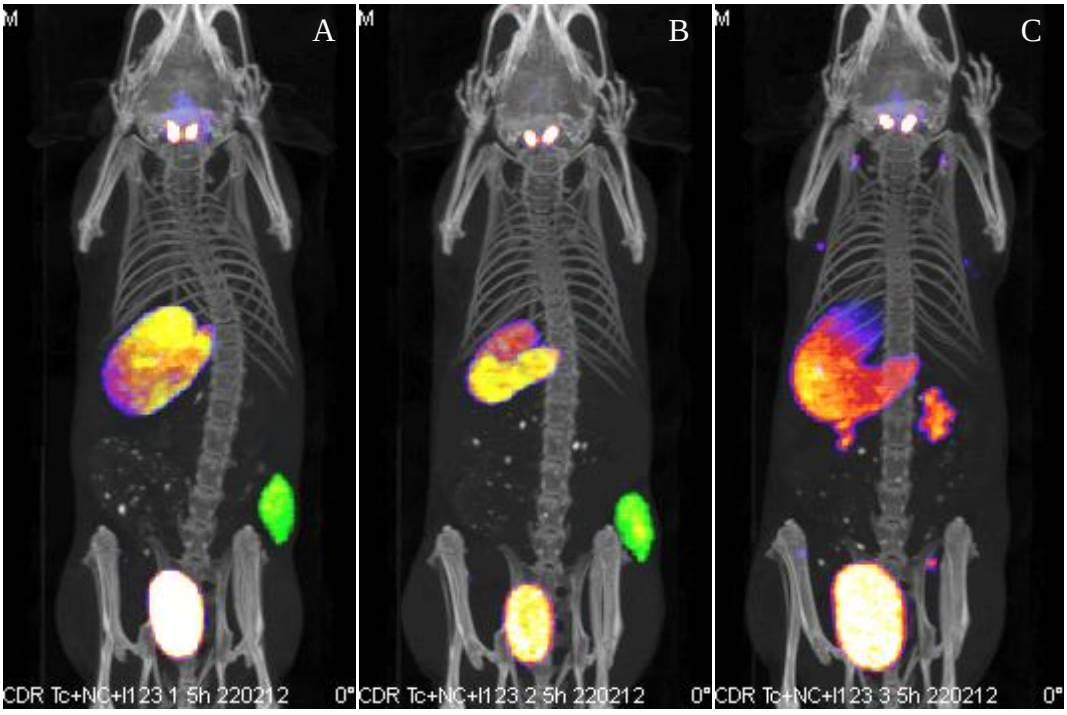

Figure 25. Dual-tracing experiment with pertechnetate/NFC implants imbedded with ^{123}I-NaI. A, B) Mice with radiolabelled NFC. C) Mouse with unlabelled NFC. The implant (green) remained intact during the whole experiment. No migration or disintegration was observed. Mice moving between the acquisitions did not affect the position or the integrity of the implant. Images were taken at 5 hour time point.

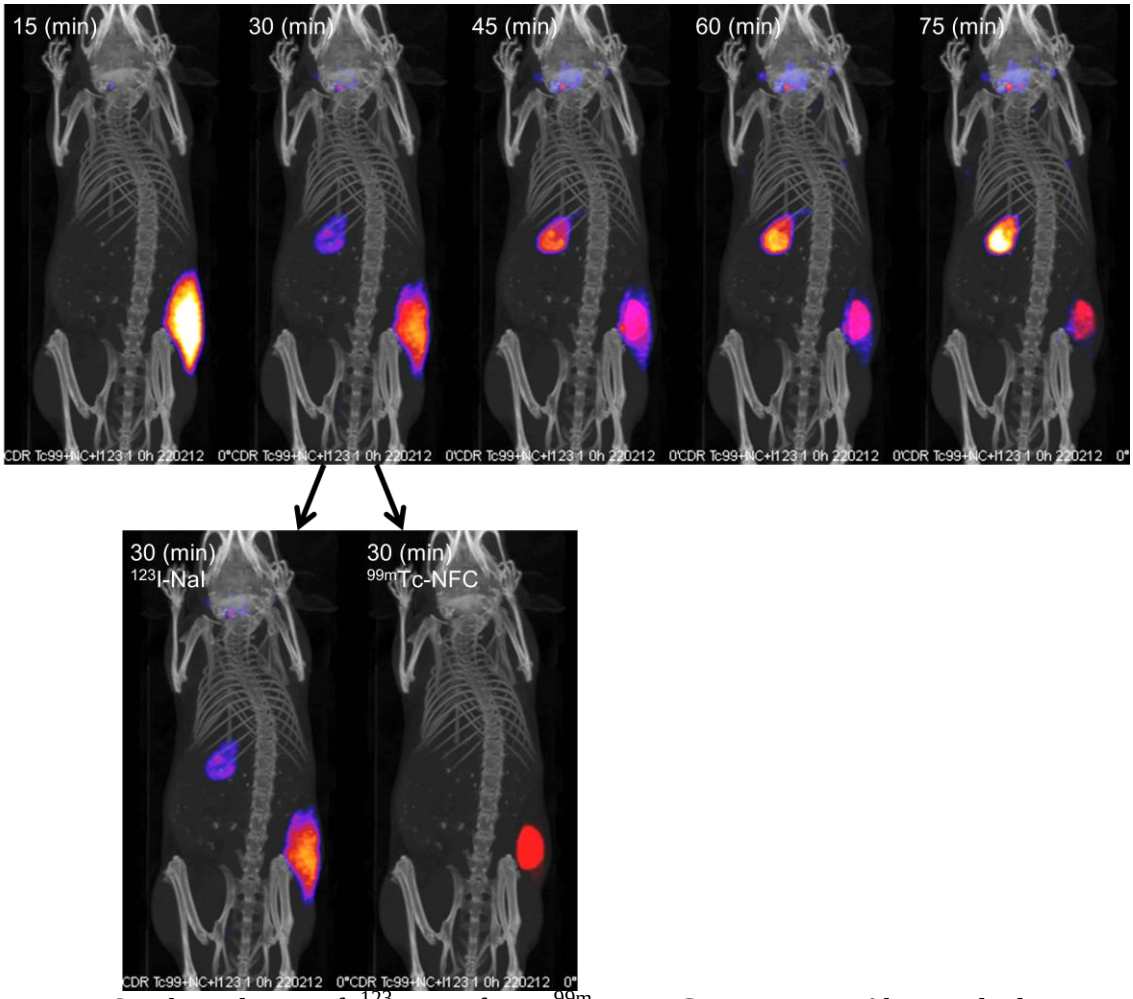

Figure 26. The release of ^{123}I-NaI from ^{99m}Tc-NFC injections. Above: dual tracing images showing implant (red) placement and test compound release. Below: 30 minute image split to visualize both radiotracers separately. ^{99m}Tc-NFC does not seem to disintegrate or absorb into the bloodstream. The NFC injections are functioning like drug releasing "implants".

7 DISCUSSION

In this study, the drug release properties of a plant-derived NFC as an injectable biomaterial were evaluated. NFC sample was imbedded with the labelled study compound for SPECT/CT imaging, in addition to dual-radionuclide tracing to confirm biomaterial positioning. Subcutaneous administration was selected as the most appropriate and convenient site for implantation.

First, the labelling of NFC with ^{99m}Tc was investigated. The results indicated that the labelling method showed a high binding rate with less than 5 % remaining unbound. For the purpose of the dual-radionuclide tracing, it is possible that the unbound technetium accumulates in thyroid glands; however the amount (and therefore the signal) remained negligible compared to ^{123}I-NaI, which is generally known to accumulate heavily into the thyroid. Stannous chloride used for the dual-radionuclide imaging is known to have a low toxicity (Winship 1988). Therefore in light of current knowledge the possibility for human use remains viable. Due to high clearance rate of tin and the relatively low concentration of stannous chloride used in this study, the risks of toxic symptoms from tin alone is very low. In addition, stannous chloride is not required if there is no need to track the material itself. Furthermore the safety of nanofibrillar cellulose has been demonstrated by numerous studies (Pitkänen et al. 2010, Vartiainen et al. 2011), which is another implication for its use as biomaterial.

It has been shown that NFC is highly biodurable (Märtson et al 1999). This suggests that the applications for a non-degrading and biocompatible material would be a long-term drug releasing biomaterial; ideal as an extended release product for chronic diseases. The steady and continuous release of drug can be achieved through formulation processes; however further studies are required for more comparative analysis.

The diffusion study of different molecular sized dextrans shows that the molecular weight and size of the compounds are contributing to the rate of passive diffusion through the nanofibrillar cellulose matrix. Dextrans as well as NFC are composed of glucose molecules and according to this study the dextrans and NFC do not show a clear chemical affinity, suggesting that the passive diffusion is limited by physical factors. If no chemical attraction is found, any smaller compounds less than 4 kDa, show a fast rate of diffusion basically unhindered by the NFC matrix. The movement of larger compounds, above 20 kDa, is hindered by nanofibrillar cellulose. Furthermore the release of dextrans is shown to be steady. This suggests that NFC might possess inherent controlled release properties for larger compounds, such as protein drugs. However, the possible chemical interactions between proteins and NFC should be

investigated individually. NFC contains many hydroxyl groups as well as some carboxyl groups which might interact with the drug compounds imbedded within the matrix; therefore making the predictions of release profiles difficult for different compounds. However, considering the current increase of interest in pharmaceutical research towards the possibilities of macromolecular protein/peptide drugs, nanofibrillar cellulose might offer a new potential method for nonparenteral delivery, as the administration of protein drugs has been one of the main challenges.

The release and distribution of ^{123}I-NaI and ^{123}I-β-CIT (cocaine analogue) from NFC implants were evaluated. Both study compounds showed rapid release from the implant as expected regarding the diffusion study with low molecular weight compounds. However ^{123}I-β-CIT shows a slightly slower release as a larger compound. Due to the rapid release, it can be determined that both compounds do not show an apparent binding to nanofibrillar cellulose itself. In addition, no differences were found between the biomaterial/study compound injections and the saline/study compound injections. This further indicates that the release of small compounds is not hindered by NFC. Rather the difference in between the release profiles of the two compounds is more likely explained by physiological properties than the properties of the biomaterial implant.

The release rate of the ^{99m}Tc-HSA was shown slower than the release rate of the smaller study compounds. In addition, a very poor absorption from the injection site into the circulation was observed; furthermore, ^{99m}Tc-HSA distributed heavily into the surrounding subcutaneous tissue. The release rate of ^{99m}Tc-HSA was steady during the whole study period; however, slower release was observed with the NFC implant injections than with the saline injections. This suggests that NFC as an injectable drug releasing biomaterial is indeed more suitable for larger compounds, such as macromolecular protein and peptide drugs. However, it is unclear if the drug release is hindered by physical factors (e.g. molecular size, molecular weight, biomaterial pore size) or chemical factors (e.g. chemical binding), as it has been shown that NFC can bind water soluble, ionizable drugs in significant quantities (Jackson et al 2011).

Furthermore this study focused mainly on physical and not chemical properties of the molecules; however NFC is known to have a slight negative surface charge (Kolakovic et al. 2012 B), thus it can be expected to have some repelling forces between the negatively charged ^{123}I-NaI and ^{99m}Tc-HSA. Indeed, the results indicate that the release of ^{123}I-NaI was more rapid from the implants than from the control saline injections. The chemical properties are more important in smaller scale, thus the repulsion forces by the negative charges are greater than the physical hindrance of the NFC matrix, which related to molecular size, a physical factor. ^{99m}Tc-HSA also has a negative charge; however the size of the molecule is considerably larger than ^{123}I-NaI, therefore the physical effect of the NFC matrix in the controlled release is more dominant. Positively charged molecules were not investigated in this study, however considering the effects of the negatively charged molecules (^{123}I-NaI and ^{99m}Tc-HSA); it is likely that a more noticeable controlled release effect would be observed with positively charged molecules.

In addition, during the study of ^{99m}Tc-HSA, it was unclear how much of the pertechnetate would label the NFC matrix while mixing the ^{99m}Tc-HSA solution with the biomaterial prior to injection. The labelling methods used were somewhat similar with both ^{99m}Tc-HSA and NFC; therefore the labelling mechanism is believed to be the same. In the case of erroneous biomaterial labelling during the study, results would show as a false positive data of slower ^{99m}Tc-HSA release from the biomaterial, as some of the NFC would be labelled instead of the ^{99m}Tc-HSA. However, during the radiochemical purity test of the ^{99m}Tc-HSA, the amount of free pertechnetate was observed very low (impurities were found below the allowed 5 %). Therefore, only the free portion of the radiolabel amongst the impurities of the total activity is theoretically able to form bonds with the biomaterial, which would still amount to much less than 5 % of the whole activity. This suggests that the ^{99m}Tc-HSA related data obtained in this study is still reliable, as the amount of possible erroneous activity detected from the biomaterial during the image acquisition is considerably lower.

The dual-radionuclide tracing SPECT/CT images show that the NFC implant has remained in its site of implantation during the whole study. In addition, autopsies were

performed to visually inspect the implants after the 24 hour study period. Intact small gel-like spheroids were found at the site of injection. The mice have been awake and moving in between acquisitions, which indicate that the NFC implant is robust enough and does not migrate within the subcutaneous tissue. Furthermore the SPECT-CT images indicate that the NFC implant does not degrade as no technetium was observed outside the site of injection, which is supported by the previous studies (Märtson et al. 1999). As a non-biodegradable material, NFC could be potentially useful as surgical tissue adhesive, space-filling injectable biomaterial for tissue repair, long-term drug delivery, and tissue engineering. However further studies are required with the use of plant-derived nanofibrillar cellulose as a biomedical device. Current problems might be concerned with the handling of the material and proper product development processes.

However, most injectable biomaterials are prepared in solution, while the gelation is triggered by an external signal, for example phototriggering (Zhang et al. 2002) or salt- and pH-sensitive self-assembly (Collier & Messersmith 2004). For nanofibrillar cellulose, a triggering mechanism is not required, as it is readily injectable in its natural state. This can prove to be advantageous in the use of biomaterials as injectable implants, as many triggers can be either toxic or challenging to perform. The ready use of NFC enables simple preparations, which in addition can lower the time and costs of the study. However handling a gel-like material can show challenges in itself. Proper mixing and accurate aspirating can prove to be more difficult than when performed with solutions.

However in the field of non-invasive and minimal invasive research, molecular imaging is a well suitable method for preclinical studies, which in this experiment, shows the potential use of NFC as a biomedical device; a drug releasing matrix. In summary, molecular imaging methods could be used to a great advantage in preclinical studies, as the data gathered related to biological processes can be done in a more meaningful matter in an intact living subject than compared to *in vitro* cell studies. However, considering the importance of current cell studies in the drug development process, molecular imaging methods should still provide invaluable supplementary data that could help discovering potential lead molecules, and to further evaluate their efficiency

and safety before clinical phases. Therefore potentially greatly reducing time and costs of the tedious development process, in addition to limiting the amount of failed new drug candidates.

8 CONCLUSIONS

This study shows a robust, simple and a reliable method of labelling NFC with ^{99m}Tc, which could prove to be useful for any further studies involving NFC and molecular imaging techniques, such as SPECT/CT. The small animal imaging was carried out successfully; however no differences were found between the NFC and saline injections for the smaller compounds ^{123}I-NaI and ^{123}I-β-CIT. Both compounds were released rapidly and sustained release was not observed with the NFC injections. However with a larger compound, ^{99m}Tc-HSA, a clear difference was found between the biomaterial and saline injections. The differences between the release kinetics could be explained by either physical or chemical interactions with NFC. Therefore, according to this study, the gel-like NFC could be more suitable for larger compounds, such as proteins or peptides, and or positively charged molecules, as NFC has a slight negative charge in neutral pH. The 1 % hydrogel was easily prepared and readily administered as an injection. In addition, the gel remained at the injection site without migrating or degrading, even after the subjects have been awake and moving. For larger compounds, NFC-hydrogel “implants” show a potential use in the biomedical field; however more studies are required for further discussion and conclusions.

ACKNOWLEDGEMENTS

I want to thank the following people who have been a great help and support during my work with this thesis. My supervisors Mari Raki and Kim Bergström, co-workers and friends Ruzica Kolakovic, Sanjay Sarkhel, Staffan Berg, and our professor Marjo Yliperttula. Thank you for your guidance, ideas and encouragement.

REFERENCES

Ahola S, Österberg M, Laine J: Cellulose nanofibrils—adsorption with poly(amideamine) epichlorohydrin studied by QCM-D and application as a paper strength additive. Cellulose 15: 303-314, 2008

Alberto R, Schibli R, Egli A, Schubiger AP, Abram U, Kaden TA: A Novel Organometallic Aqua Complex of Technetium for the Labeling of Biomolecules: Synthesis of [99m Tc(OH 2) 3 (CO) 3] + from [99m TcO 4] - in Aqueous Solution and Its Reaction with a Bifunctional Ligand. J Am Chem Soc 120: 7987-7988, 1998

Andros G, Harper PV, Lathrop KA: Pertechnetate-99m localization in man with applications to thyroid scanning and the study of thyroid physiology. J Clin Endocrinol Metab 25: 1067-1076, 1965

Beekman FJ, Vastenhouw B: Design and simulation of a high-resolution stationary SPECT system for small animals. Phys med Biol 49: 4579, 2004

Beekman F, van der Have F: The pinhole: gateway to ultra-high-resolution three-dimensional radionuclide imaging. Eur J Nucl Med Mol Imaging 34: 151-161, 2007

Beyer T, Townsend DW, Brun T, Kinahan PE, Charron M, Roddy R, Jerin J, Young J, Byars L, Nutt R: A combined PET/CT scanner for clinical oncology. J Nucl Med 41: 1269-1279, 2000

Bhattacharya M, Malinen MM, Lauren P, Lou YR, Kuisma SW, Kanninen L, Lille M, Corlu A, Guguen-Guillouzo C, Ikkala O, Laukkanen A, Urtti A, Yliperttula M: Nanofibrillar cellulose hydrogel promotes three-dimensional liver cell culture. J Control Release: published online Jul 7, 2012

Bodin A, Ahrenstedt L, Fink H, Brumer H, Risberg B, Gatenholm P: Modification of nanocellulose with a xyloglucan-RGD conjugate enhances adhesion and proliferation of endothelial cells: implications for tissue engineering. Biomacromolecules 8: 3697-3704, 2007

Bonné MJ, Galbraith E, James TD, Wasbrough MJ, Edler KJ, Jenkinks ATA, Helton M, McKee A, Thielemans W, Psillakis E, Marken F: Boronic acid dendrimer receptor modified nanofiblrillar cellulose membranes. J Mater Chem 20: 588-594, 2010

Booij J, Habraken JB, Bergmans P, Tissingh G, Winogrodzka A, Wolters EC, Janssen AG, Stoof JC, van Royen EA: Imaging of dopamine transporters with iodine-123-FP-CIT SPECT in healthy controls and patients with Parkinson's disease. J Nucl Med 39: 1879-1984, 1998

Borges AC, Eyholzer C, Duc F, Bourban PE, Tingaut P, Zimmermann T, Pioletti DP, Månson JA: Nanofibrillated cellulose composite hydrogel for the replacement of the nucleus pulposus. Acta Biomat 9: 3412-3421, 2011

Buxton DB, Antman M, Danthi N, Dilsizian V, Fayad ZA, Garcia MJ, Jaff MR, Klimas M, Libby P, Nahrendorf M, Sinusas AJ, Wickline SA, Wu JC, Bonow RO, Weissleder R: Report of the National Heart, Lung, and Blood
Institute working group on the translation of cardiovascular molecular imaging. Circulation 123: 2157-2163, 2011

Buzea C, Pacheco Blandino II, Robbie K: Nanomaterials and nanoparticles: sources and toxicity. Biointerphases 2: MR17-MR71, 2007

Bäckdahl H, Helenius G, Bodin A, Nannmark U, Johansson BR, Risberg B, Gatenholm P: Mechanical properties of bacterial cellulose and interactions with smooth muscle cells. Biomaterials 27: 2141-2149, 2006

Cherian BM, Leão AL, de Souza SF, Costa LMM, de Olyveira GM, Kottaisamy M, Nagarajan ER, Thomas S: Cellulose nanocomposites with nanofibres isolated from pineapple leaf fibers for medical applications. Carbohyd Polym 86: 1790-1798, 2011

Cherry SR: Multimodality in vivo imaging systems: twice the power or double the trouble. Annu Rev Biomed Eng 8: 35-62, 2006

Cherry SR: Multimodality imaging: Beyond PET/CT and SPECT/CT. Semin Nucl Med 39: 348-353, 2009

Clasen C, Sultanova B, Wilhelms T, Heisig P, Kulicke W-M: Effects of Different Drying Processes on the Material Properties of Bacterial Cellulose. Macromol Symp 244: 48-58, 2006

Collier JH, Messersmith PB: Self-assembling polymer-peptide conjugates: nanostructural tailoring. Adv Mater 16: 907-910, 2004

Cuaron JJ, Hirsch AE, Medich DC, Hirsch JA, Rosenstein BS: Introduction to radiation safety and monitoring. J Am Coll Radiol 8: 259-264, 2011

Di Carli MF, Hachamovitch R: Should PET replace SPECT for evaluating CAD? The end of the beginning. J Nucl Cardiol 13: 2-7, 2006

Dinand E, Chanzy H, Vignon MR: Parenchymal cell cellulose from sugar beet pulp: preparation and properties. Cellulose 3: 183-188, 1996

Donnelly EH, Nemhauser JB, Smith JM, Kazzi ZN, Farfán EB, Chang AS, Naeem SF: Acute radiation syndrome: assessment and management. South Med J 103: 541-546, 2010

Eichhorn SJ, Baillie CA, Zafeiropoulos N, Mwaikambo LY, Ansell MP, Dufresne A, Entwistle KM, Herrera-Franco PJ, Escamilla GC, Groom LH, Hughes M, Hill C, Rials TG, Wild PM: Current international research into cellulosic fibres and composites. J Mat Sci 36: 2107-2131, 2001

European Comission: Council of the European Union in the Council Directive 96/29/Euratom: Basic safety standards for the protection of the health of workers and the general public against the dangers arising from ionizing radiation. 13.5.1996

European Comission: Council of the European Union in the Council Directive 86/609/EEC: Protection of animals used for experimental and other scientific purposes. 24.11.1986

Eyholzer C, Borges AC, Duc F, Bourban PE, Tingaut P, Zimmermann T, Ma□nson JAE, Oksman K: Biocomposite Hydrogels with Carboxymethylated, Nanofibrillated Cellulose Powder for Replacement of the Nucleus Pulposus. Biomacromolecules 12: 1419-1427, 2011

Fueger BJ, Czernin J, Hildebrandt I, Tran C, Halpern BS, Stout D, Phelps ME, Weber WA: Impact of animal handling on the results of 18F-FDG PET studies in mice. J Nucl Med 47: 999-1006, 2006

Fusco MA, Peek NF, Jungerman JA, Zielinski FW, DeNardo SJ, Denardo GL: Production of Carrier-Free ^{123}I Using the ^{127}I(p,5n)^{123}Xe Reaction. J Nucl Med 13: 729-732, 1972

Gilkes NR, Henrissat B, Kilburn DG, Miller RC jr, Warren RA: Domains in microbial beta-1, 4-glycanases: sequence conservation, function and enzyme families. Microbiol Rev 55: 303-315, 1991

Goetz C, Breton E, Choquet P, Israel-Jost V, Constantinesco A: SPECT low-field MRI system for small-animal imaging. J Nucl Med 49: 88-93, 2008

Guo H, Yang J, Gallazzi F, Prossnitz ER, Sklar LA, Miao Y: Effect of DOTA position on melanoma targeting and pharmacokinetic properties of 111In-labeled lactam bridge-cyclized alpha-melanocyte stimulating hormone peptide. Bioconjug Chem 20: 2162-2168, 2009

Hasegawa BH, Gingold EL, Reilly SM, Liew S-C, Cann CE: Description of a simultaneous emission-transmission CT system. Medical Imaging IV: Image Formation 50, 1990

Henriksson M, Berglund LA, Isaksson P, Lindström T, Nishino T: Cellulose nanopaper structures of high toughness. Biomacromolecules 9: 1579-1585, 2008

Hildebrandt IJ, Su H, Weber WA: Anesthesia and other considerations for in vivo imaging of small animals. ILAR J 49: 17-26, 2008

Hirschmann MT, Wagner CR, Rasch H, Henckel J: Standardized volumetric 3D-analysis of SPECT/CT imaging in orthopaedics: overcoming the limitations of qualitative 2D analysis. BMC Medical Imaging 12: 5, 2012

Hu Y, Catchmark JM: Effect of freeze-drying behavior on the density and structure of bacterial cellulosic films by different acidic and alkaline treatments. American Society of Agricultural and Biological Engineers, Reno, Nevada, June 21 - June 24, 2009

Hui J, Yuanyuan J, Jiao W, Yuan H, Yuan Z, Shiru J: Potentiality of Bacterial Cellulose as the Scaffold of Tissue Engineering of Cornea. International Conference on BioMedical Engineering and Informatics: 1-5, 2009

Hutchens SA, Benson RS, Evans BR, O'neill HM, Rawn CJ: Biomimetic synthesis of calcium-deficient hydroxyapatite in a neutral hydrogel. Biomaterials 27: 4661-4670, 2006

The International Commission on Radiological Protection: The 2007 recommendations of the international commission on radiological protection. ICPR publication 103. Ann ICRP 37(2-4), 2007

Jackson JK, Letchford K, Wasserman BZ, Ye L, Hamad WY, Burt HM: The use of nanocrystalline cellulose for the binding and controlled release of drugs. Int J Nanomedicine 6: 321-330, 2011

Jaszczak RJ, Coleman JR, Whitehead FR: Physical factors affecting quantitative measurements using gamma camera-based single photon emission computed tomography (SPECT). IEEE Trans Nucl Sci 28: 69-80, 1981

Jeon J-H, Oh I-K, Kee C-D, Kim S-J: Bacterial cellulose actuator with electrically driven bending deformation in hydrated condition. Sens Act B 146: 307-313, 2010

Jung R, Jin HJ: Preparation of Silk Fibroin/Bacterial Cellulose Composite Films and their Mechanical Properties. Key Eng Mater 342-343: 741-744, 2007

Karp JS, Surti S, Daube-Witherspoon ME, Muehllehner G: Benefit of time-of-flight in PET: experimental and clinical results. J Nucl Med 49: 462-470, 2008

Keidar Z, Israel O, Krausz Y: SPECT/CT in tumor imaging: technical aspects and clinical applications. Sem Nucl Med 33: 205-218, 2003

Klemm D, Heublein B, Fink HP, Bohn A: Cellulose: fascinating biopolymer and sustainable raw material. Angew Chem Int Ed Engl 44: 3358-3393, 2005

Klemm D, Schumann D, Kramer F, Heßler, Hornung M, Schmauder H-P, Marsch S: Nanocelluloses as innovative polymers in research and applications. Adv Polym Sci 205: 49-96, 2006.

Klemm D, Schumann D, Kramer F, Heßler, Koth D, Sultanova B: Nanocellulose materials – different cellulose, different functionality. Macromol Symp 280: 60-71, 2009

Klemm D, Kramer F, Moritz S, Lindström T, Ankerfors M, Gray D, Dorris A: Nanocelluloses: a new family of nature-based materials. Angew Chem Int 50: 5438-5466, 2011

A) Kolakovic R, Laaksonen T, Peltonen L, Laukkanen A, Hirvonen J: Spray-dried nanofibrillar cellulose microparticles for sustained drug release. Int J Pharm 430: 47-55, 2012

B) Kolakovic R, Peltonen L, Laukkanen A, Hirvonen J, Laaksonen T: Nanofibrillar cellulose films for controlled drug delivery. Eur J Pharm Biopharm 82: 308-315, 2012

Korhonen JT, Kettunen M, Ras RH, Ikkala O: Hydrophobic nanocellulose aerogels as floating, sustainable, reusable, and recyclable oil absorbents. ACS Appl Mater Interfaces 3: 1813-1816, 2011

Kraitchman DL, Tatsumi M, Gilson WD, Ishimori T, Kedziorek D, Walczak P, Segars WP, Chen HH, Fritzges D, Izbudak I, Young RG, Marcelino M, Pittenger MF, Solaiyappan M, Boston RC, Tsui BM, Wahl RL, Bulte JW: Dynamic imaging of allogeneic mesenchymal stem cells trafficking to myocardial infarction. Circulation 112: 1451-1461. 2005.

Kung AL, Zabludoff SD, France DS, Freedman SJ, Tanner EA, Vieira A, Cornell-Kennon S, Lee J, Wang B, Wang J, Memmert K, Naegeli HU, Petersen F, Eck MJ, Bair KW, Wood AW, Livingston DM: Small molecule blockade of transcriptional coactivation of the hypoxia-inducible factor pathway. Cancer Cell 6: 33-43, 2004

Laaksonen P, Walther A, Malho JM, Kainlauri M, Ikkala O, Linder MB: Genetic engineering of biomimetic nanocomposites: diblock proteins, graphene, and nanofibrillated cellulose. Angew Chem Int Ed Engl 50: 8688-8691, 2011

Linder Å, Gatenholm P: Effect of cellulose substrate on assembly of xylans. In book Hemicelluloses: Science and Technology, chapter 16: 236-253. Gatenholm P, Tenkanen M (eds). American Chemical Society, 2004

Mandel SJ, Shankar LK, Benard F, Yamamoto A, Alavi A: Superiority of iodine-123 compared with iodine-131 scanning for thyroid remnants in patients with differentiated thyroid cancer. Clin Nucl Med 26: 6-9, 2001

Maneerung T, Tokura S, Rujiravanit R: Impregnation of silver nanoparticles into bacterial cellulose for antimicrobial would dressing. Carbohyd Polym 72: 43-51, 2008

Mariani G, Bruselli L, Kuwert T, Kim EE, Flotats A, Israel O, Dondi M, Watanabe N: A review on the clinical uses of SPECT/CT. Eur J Nucl Med Mol Imaging 37: 1959-1985, 2010

Marzola P, Osculati F, Sbarbati A: High field MRI in preclinical research. Eur J Radiol 48: 165-170, 2003

Massoud TF, Gambhir SS: Molecular imaging in living subjects: seeing fundamental biological processes in a new light. Genes Dev 17: 545-580, 2003

A) Mathew AP, Oksman K, Pierron D, Harmad M-F: Crosslinked fibrous composites based on cellulose nanofibers and collagen with in situ pH induced fibrillation. Cellulose 19: 139-150, 2012

B) Mathew AP, Oksman K, Pierron D, Harmad M-F: Fibrous cellulose nanocomposite scaffolds prepared by partial dissolution for potential use as ligament or tendon substitutes. Carbohyd Polym 87: 2291-2298, 2012

McElroy DP, MacDonald LR, Beekman FJ, Yochuan W, Patt BE, Iwanczyk JS, Tsui BMW, Hoffman EJ: Performance evaluation of A-SPECT: a high resolution desktop pinhole SPECT system for imaging small animals. IEEE Trans Nucl Sci 49: 2139-2147, 2002

Merkel OM, Librizzi D, Pfestroff A, Schurrat T, Béhé M, Kissel T: In vivo SPECT and real-time gamma camera imaging of biodistribution and pharmacokinetics of siRNA delivery using an optimized radiolabeling and purification procedure. Bioconjug Chem 20: 174-182, 2009

Miyamoto T, Takahashi S, Ito H, Inagaki H, Noishiki Y: Tissue biocompatibility of cellulose and its derivatives. J Biomed Mater Res 23: 125-133, 1989

Ministry of Agriculture and Forestry: Animal Welfare Act (247/1996)

Ministry of Agriculture and Forestry: ELLA – Finnish National Animal Experiment Board, Act on the Use of Animals for Experimental Purposes (62/2006)

Ministry of Social Affairs and Health: STUK – Radiation and Nuclear Safety Authority (Finland), Radiation Act 27.3.1991/592 27.3.1991

Mouse Genome Consortium: Initial sequencing and comparative analysis of the mouse genome. Nature 420: 520-562, 2002

Märtson M, Viljanto J, Hurme T, Laippala P, Saukko P: Is cellulose sponge degradable or stable as implantation material? An in vivo subcutaneous study in the rat. Biomaterials 20: 1989-1995, 1999

Narra VR, Howell RW, Harapanhalli RS, Sastry KSR, Rao DV: Radiotoxicity of some iodine-123, iodine-125 and iodine-131-labeled compounds in mouse testes: implications for radiopharmaceutical design. J Nucl Med 33: 2196-2201, 1992

O'Tuama LA, Treves ST, Larar JN, Packard AB, Kwan AJ, Barnes PD, Scott RM, Black PM, Madsen JR, Goumnerova LC, Sallan SE, Tarbell NJ: Thallium-201 versus technetium-99m-MIBI SPECT in evaluation of childhood brain tumors: a within-subject comparison. J Nucl Med 34: 1045-1051, 1993

Pass B, Baranov AE, Kleshchenko ED, Aldrich JE, Scallion PL, Gale RP: Collective biodosimetry as a dosimetric "gold standard": a study of three radiation accidents. Health Phys 72: 390-396, 1997

Pichler BJ, Judenhofer MS, Catana C, Walton JH, Kneilling M, Nutt RE, Siegel SB, Claussen CD, Cherry SR: Performance test of an LSO-APD detector in a 7-T MRI scanner for simultaneous PET/MRI. J Nucl Med 47: 639-647, 2006

Pitkänen M, Sneck A, Hentze H-P, Sievänen J, Hiltunen J, Hellén E, Honkalampi U, von Wright A: Nanofibrillarcellulose –Assessment of cytotoxicand genotoxicproperties in vitro. 2010 Intl Conf on Nanotechnology for the Forest Products Ind, Sep 27-29, 2010

Pääkkö M, Ankerfors M, Kosonen H, Nykänen A, Ahola S, Osterberg M, Ruokolainen J, Laine J, Larsson PT, Ikkala O, Lindström T: Enzymatic hydrolysis combined with mechanical shearing and high-pressure homogenization for nanoscale cellulose fibrils and strong gels. Biomacromolecules 8: 1934-1941, 2007

Rahmim A, Zaidi H: PET versus SPECT: strengths, limitations and challenges. Nucl Med Commun 29: 193-207, 2008

Rowland DJ, Cherry SR: Small-animal preclinical nuclear medicine instrumentation and methodology. Semin Nucl Med 38: 209-222, 2008

Schade JH, Hoving J, Brouwers JR, Riedstra-van Gent HG, Zijlstra J, Dijkstra JP: Technetium-99m carboxymethylcellulose: a newly developed fibre marker for gastric emptying studies. Eur J Nucl Med 18: 380-384, 1991

Schellingerhout D, Accorsi R, Mahmood U, Idoine J, Lanza RC, Weissleder R: Coded aperture nuclear scintigraphy: a novel small animal imaging technique. Mol Imaging 1: 344-353, 2002

Sharp P, Gemmel P, Cherryman G, Besson J, Crawford J, Smith F: Application of iodine-123-labeled isopropylamphetamine imaging to the study of dementia. J Nucl Med 27: 761-768, 1986

Sharp TL, Dence CS, Engelbach JA, Herrero P, Gropler RJ, Welch MJ: Techniques necessary for multiple tracer quantitavie small-animal imaging studies. Nucl Med Biol 32: 875-884, 2005

Shimotoyodome A, Suzuki J, Kumamoto Y, Hase T, Isogai A: Regulation of postprandial blood metabolic variables by TEMPO-oxidized cellulose nanofibers. Biomacromolecules 12: 3812-3818, 2011

Shultz LD, Ishikawa F, Greiner DL: Humanized mice in translational biomedical research. Nature Rev Immunol 7: 118-130, 2007

Siró I, Plackett D: Microfibrillated cellulose and new nanocomposite materials: a review. Cellulose 17: 459-494, 2010

Stodilka RZ, Blackwood KJ, Prato FS: Tracking transplanted cells using dual-radionuclide SPECT. Phys Med Biol 51: 2619-2632, 2006

Soundararajan A, Bao A, Phillips WT, Perez R 3rd, Goins BA: [(186)Re]Liposomal doxorubicin (Doxil): in vitro stability, pharmacokinetics, imaging and biodistribution in a head and neck squamous cell carcinoma xenograft model. Nucl Med Biol 36: 515-524, 2009

Thrall JH, Freitas JE, Swanson D, Rogers WL, Clare JM, Brown ML, Pitt B: Clinical comparison of cardiac blood pool visualization with technetium-99m red blood cells labeled in vivo and with technetium-99m human serum albumin. J Nucl Med 19: 796-803, 1978

Toyama H, Ichise M, Liow JS, Vines DC, Seneca NM, Modell KJ, Seidel J, Green MV, Innis RB: Evaluation of anesthesia effects on [18F]FDG uptake in mouse brain and heart using small animal PET. Nucl Med Biol 31: 251-256, 2004

Traggiai E, Chicha L, Mazzucchelli L, Bronz L, Piffaretti J-C, Lanzavecchia A, Manz MG: Development of a Human Adaptive Immune System in Cord Blood Cell-Transplanted Mice. Science 304: 104-107, 2004

United Nations Scientific Committee on the Effects of Atomic Radiation: UNSCEAR 2006 Report: Effects of Ionizing Radiation. United Nations, 2006

Valo H, Kovalainen M, Laaksonen P, Häkkinen M, Auriola S, Peltonen L, Linder M, Järvinen K, Hirvonen J, Laaksonen T: Immobilization of protein-coated drug nanoparticles in nanofibrillar cellulose matrices--enhanced stability and release. J Control Release 156: 390-397, 2011

Vartiainen J, Pöhler T, Sirola K, Pylkkänen L, Alenius H, Hokkinen J, Tapper U, Lahtinen P, Kapanen A, Putkisto K, Hiekkataipale P, Eronen P, Ruokolainen J, Laukkanen A: Health and environmental safety aspects of friction grinding and spray drying of microfibrillatedcellulose. Cellulose 18: 775-786, 2011

Vitta S, Thiruvengadam V: Multifunctional bacterial cellulose and nanoparticle-embedded composites. Curr Sci 102: 1398-1405, 2012

Wackers FJT, Berman DS, Maddahi J, Watson DD, Beller GA, Strauss HW, Boucher CA, Picard M, Holman BL, Fridrich R, Inglese E, Delaloye B, Bischof-Delaloye A, Camin L, McKusick K: Technetium-99m Hexakis 2-Methoxyisobutyl Isonitrile:Human Biodistribution, Dosimetry, Safety, and Preliminary Comparison to Thaffium-201 for Myocardial Perfusion Imaging. J Nucl Med 30: 301-311, 1989

Wiegand C, Elsner P, Hipler U-C, Klemm D: Protease and ROS activities influenced by a composite of bacterial cellulose and collagen type I in vitro. Cellulose 13: 689-698, 2006

Willmann JK, van Bruggen N, Dinkelborg LM, Gambhir SS: Molecular imaging in drug development. Nat Rev Drug Discov 7: 591-607, 2008

Zaidi H, Hasegawa B: Determination of the attenuation map in emission tomography. J Nucl Med 44: 291-315, 2003

Zhang ZY, Shum P, Yates M, Messersmith PB, Thompson DH: Formation of fibrinogen-based hydrogels using phototriggerable diplasmalogen liposomes. Bioconjug Chem 13: 640-646, 2002

Zhang SJ, Wu JC: Comparison of imaging techniques for tracking cardiac stem cell therapy. J Nucl Med 48: 1916-1919, 2007